Nuclear-Magnetic-Resonance Study of Impurity Effects in a Heisenberg Antiferromagnet

M. BUTLER* AND V. JACCARINO*
Physics Department, University of California, Santa Barbara, California 93106

AND

N. KAPLAN*†
Physics Department, University of California, Santa Barbara, California 93106
and
Physics Department, Hebrew University, Jerusalem, Israel

AND

H. J. GUGGENHEIM
Bell Telephone Laboratories, Murray Hill, New Jersey 07971

(Received 4 November 1969)

Experimental and theoretical impurity-magnon-mode studies have been made using the F^{19} NMR in the impure antiferromagnet $MnF_2:X$ (where $X=$V, Fe, Co, Ni, or Zn, usually in concentrations of 1% or less). Fixed-frequency spin-echo techniques were employed with a variable external field applied parallel to the unique axis. At low temperatures, the frequency position and relative intensity of a given, discrete impurity-associated F^{19} resonance were used to identify the position in the lattice of that particular F^- ion relative to the impurity. Both the homogeneous and inhomogeneous linewidths of these resonances were examined, and their magnitudes were interpreted. From the temperature dependence of the many resonances associated with a specific impurity, the temperature dependence of the impurity, near-neighbor (nn), and next-near-neighbor (nnn) spin magnetizations $M_i(t)$ could be determined. It was found that a sizable nn host-impurity exchange interaction J_{nn} is required to fit the $M_i(t)$ data in the $MnF_2:X$, whereas in pure MnF_2 and FeF_2, $|J_{nn}|\ll|J_{nnn}|$. Good agreement between experiment and the Hone-Walker (HW) thermodynamic Green's-function theory was found for $M_{nnn}(T)$ for the case of a spinless impurity (Zn^{2+}); a corresponding theory does not yet exist for which both $S_{imp}\neq 0$ and $J_{nn}\neq 0$. From the field dependence of the F^{19} resonances in MnF_2:Zn at elevated temperatures, the parallel susceptibility $\chi_{nnn}''(T)$ of a nnn to a spinless impurity was determined. Experiment and a modified spin-wave theory, which uses the HW impurity spectral weight function, agree well. The magnitude and temperature dependence of the nuclear spin-lattice relaxation rates $(T_1)_i^{-1}$ for several of the impurity-associated F^{19} resonances was measured. Using the same theoretical approach as was made for $\chi_i''(T)$, the nuclear relaxation via two-magnon scattering was obtained. Comparison between theory and experiment is not possible, as this requires a detailed knowledge of the spatial dependence of the phase of the impurity-magnon wave functions which are unknown at present. In addition to the single-impurity studies, several crystals with larger impurity concentrations were examined. Their resonances gave information on the tendency of impurities to cluster. Finally, a detailed, albeit crude, model of strain effects on the local F^{19} transferred hyperfine fields in an imperfect MnF_2 crystal is given, which yields reasonable results for the displacements of specific resonances from their expected positions.

I. INTRODUCTION

As recently as 15 years ago most of the experimental information we had of the ground state and thermodynamic properties of magnetically ordered systems was derived from macroscopic measurements (e.g., susceptibility and specific heat). The subsequent application of microscopic techniques (e.g., inelastic neutron scattering and hyperfine field studies) has provided more detailed and precise data to the extent that meaningful comparisons between experiment and more sophisticated theories are becoming ever more commonplace. For example, NMR studies in Heisenberg ferromagnets and antiferromagnets have shown that the interaction between magnons causes measurable deviations from the predictions of linear spin-wave theory of the temperature dependence of the magnetization.[1]

However, the full power of hyperfine field studies to probe the magnetic solid was not realized until impurities were added to an otherwise perfect system. In ferromagnetic alloys, for instance, Mössbauer-effect and NMR experiments showed that the magnetizations of impurity, its nearest neighbors and the host might well have different temperature dependencies (e.g., Mn in Fe).[2] Unfortunately, despite their fundamental importance, both the origins of the hyperfine fields and the nature of exchange interactions and impurity states in ferromagnetic transition metals is presently so poorly understood that what little progress has been made is subject to much controversy.

The situation with regard to insulating ferro- and

* Supported in part by the National Science Foundation.
† Present address: Physics Department, Hebrew University, Jerusalem, Israel.

[1] G. G. Low, Proc. Phys. Soc. (London) **82**, 992 (1963).
[2] Y. Koi, A. Tsujimura, and T. Hihara, J. Phys. Soc. (Japan) **19**, 1493 (1964).

antiferromagnets is quite different. A proper theory of the elementary excitations from the ground state exists and has been experimentally verified for the perfect crystal.[3] When impurities are added, a very definite assignment to the impurity spin and its near-neighbor exchange interaction may be given. Furthermore, studies of the optical spectra[4] and inelastic scattering of neutrons[5] have revealed much detail concerning impurity spin-wave modes and, in particular, the magnitude of the impurity-host exchange coupling. Some of the most fruitful investigations have been made on MnF_2:X, where X is a transition-metal impurity ion. From the viewpoint of resonance techniques this is an ideal antiferromagnet. The F^{19} NMR is easy to detect, unfettered with quadrupolar effects ($I^{19}=\frac{1}{2}$, 100% abundant) and has been studied in elaborate detail in the pure crystal MnF_2,[6] perhaps the best understood antiferromagnet. The ability of the F^{19} NMR to probe the degree of localization of the impurity modes has been exploited in the present work and was, in fact, the motivation for these undertakings.

In Sec. II we review certain features of pure MnF_2 and the impure system as are necessary to understand local site symmetries, the contributions to the local field and magnetic ordering. A brief description of the sample preparation, orientation, and resonance techniques employed is given. Section III outlines the origins and identification of the numerous resonances that are seen (extrapolated to 0°K), discusses their linewidths and T_2's, and correlates these properties with the spin of the particular impurity under investigation. Section IV gives the observed temperature dependencies of the various resonances and relates these to the temperature dependence of the impurity, near-neighbor (nn), next-near-neighbor (nnn), and host magnetizations. The experimental results on the susceptibility of a nnn to a nonmagnetic impurity are reported. Measurements of the nuclear spin-lattice relaxation time T_1 for impurity associated resonances are given. Finally, interpretations of the behavior of the magnetizations, susceptibility, and T_1 are given based on different model theories. In the Appendix a theory is outlined for explaining the effects that strains, caused by the insertion of an impurity, have on the line positions and widths.

II. CRYSTAL STRUCTURE AND EXPERIMENTAL PROCEDURE

A. Crystal and Magnetic Structure

MnF_2 has the rutile structure shown in Fig. 1. The Mn^{2+} ions form a body-centered tetragonal lattice.

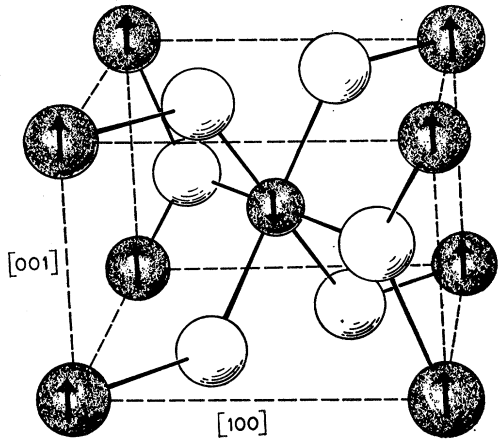

FIG. 1. The crystal and magnetic structure of antiferromagnetic MnF_2. The shaded balls represent Mn^{2+} ions, with the arrows indicating the directions of the electronic spin magnetization on the two sublattices. The unshaded balls represent the intervening F^- ions.

Below the ordering temperature ($T_N=67$°K) the Mn spins form a simple two sublattice antiferromagnet with the spins at corner and body-centered positions oppositely directed, parallel to the unique or c axis. The dominant exchange interaction J_2 is between nnn magnetic ions at the corner and body-centered positions and is antiferromagnetic. Rather surprisingly the nn interaction J_1 between adjacent spins along the c axis is much weaker and ferromagnetic.[7]

There are two physically inequivalent F sites. Shown in Fig. 2 is the position and orientation of the three nn Mn spins relative to one of these. Its counterpart has the same local environment with the direction of the spins reversed. The application of a magnetic field parallel to the c axis enables one to distinguish the two sites by observation of the field dependence of the

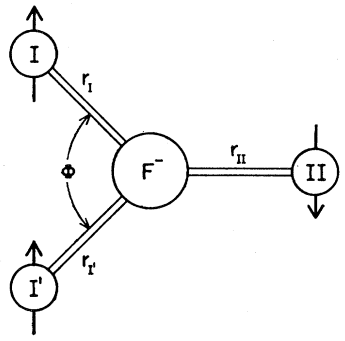

FIG. 2. The F^- ion local site symmetry in MnF_2 in the (110) plane. Below T_N the electronic spin magnetizations of Mn^{2+} ions labeled I, I′, and II are aligned parallel to the c axis, as indicated by the arrows. For an equivalent F^- ion in the (1$\bar{1}$0) plane the nearest-neighbor magnetizations are oppositely directed to those shown in the figure. The major part of local field at a given F^{19} nucleus results from the transferred hyperfine interaction with these nearest-neighbor magnetic ions.

[3] For a detailed review see the article by F. Keffer, in *Handbuch der Physik* (Springer-Verlag, Berlin, 1968), Vol. 18.

[4] For example, see L. F. Johnson, R. E. Dietz, and H. J. Guggenheim, Phys. Rev. Letters **17**, 13 (1966).

[5] T. M. Holden, R. A. Cowley, and W. J. L. Buyers, Solid State Commun. **6**, 145 (1968).

[6] Review article by V. Jaccarino, in *Magnetism*, edited by G. T. Rado and H. Suhl (Academic Press Inc., New York, 1963), Vol. 2A, Chap. 5.

[7] A. Okazaki, K. C. Turberfield, and R. W. H. Stevenson, Phys. Letters **8**, 9 (1964).

F^{19} NMR. This feature is important to the interpretation of the resonance spectra in the impure crystal, as we shall see.

Divalent transition-metal ion impurities enter the lattice substitutionally for the Mn^{2+} ions. For all of the magnetic impurities investigated (Fe, Co, Ni, and V) the host-impurity exchange interaction J_2' between an impurity spin and its 8 nnn is antiferromagnetic. Although the host-impurity exchange interaction J_1' between an impurity spin and its two nn has been determined by our experiments to be neither small nor always of one sign, the collective effect of having a smaller number of interacting pairs for the nn results in the orientation of the impurity spin being identical to that of the host spin it replaces.

B. Preparation and Orientation of Crystals

1. Preparation of Impurity-Doped Samples

The various iron group fluorides are prepared by reacting the highest-purity metals with 48% hydrofluoric acid. The fluorides are then dried and melted in a dry HF atmosphere at 1000°C. Single crystals of MnF_2 doped with divalent Fe, Ni, Co, Zn, or V are grown in a carbon boat using a horizontal zone melting technique. A platinum tube, used to contain the boat in a continuous flow of HF, travels through a resistance heater with a narrow hot zone at rates between 0.2 and 1.0 cm/h. The appropriate impurity fluoride is added along the zone boat before the final zone pass. In the case of Fe, Co, and Zn the distribution coefficients are very close to unity therefore the samples are generally homogeneous. However, when Ni or V is used as an impurity the samples are formed with concentration gradients. This is avoided by adding the impurity fluoride disproportionately along the zone boat to allow for the slight segregation. The resulting impurity concentrations are determined by NMR as is described in Sec. II C.

2. Orientation of Crystals

For our NMR studies the proper orientation of a sample is important as small misalignments may lead to significant errors in the extrapolation of the resonant frequencies to zero external field and the quantities derived therefrom. The initial c-axis determination is performed optically using crossed polaroids. The sample is then mounted on a holder whose axis of rotation is perpendicular to the c axis and to the magnetic field $\mathbf{H}_0$. Final orientation of the c axis relative to $\mathbf{H}_0$ is accomplished using the F^{19} NMR. For a fixed frequency the lowest applied field at which resonance is observed occurs when the sample is oriented with the applied field parallel to the c axis. Misorientation leads to a field-dependent shift

$$\Delta H=[H_0^2+H_{\rm hf}^2-2H_0H_{\rm hf}\cos\theta]^{1/2}-[H_{\rm hf}+H_0], \quad (1)$$

where H_0 is the applied field, $H_{\rm hf}$ is the hyperfine field, and θ is the misorientation angle. It is evident from examination of this expression that meaningful NMR susceptibility measurements (see Sec. IV) require sample alignment to within $\pm 1°$.

C. Resonance Techniques

All of our measurements utilized the spin-echo technique in the frequency range 130–250 MHz. The rf pulses were provided by an AML[8] Pulsed Signal Source with the pulse sequence generated by a Tektronix logic system. Detection of the nuclear signal was accomplished using a commercial T.V. tuner modified to extend its frequency range and an Arenberg Wideband Amplifier[9] as the i.f. section. Signal averaging necessary for the weaker resonances was performed by a P.A.R. Boxcar Integrator.[10] Both the transmitter and the receiver were connected through an impedance matching network to a single coil wrapped around the sample. This provided a maximum rf field inside the sample of $\sim$100 G and sufficient sensitivity for detection of the weaker resonances. Temperatures of 1.2–4.2°K and 13.9–20.3°K were achieved by pumping on liquid helium and hydrogen, respectively, with the sample immersed in the refrigerant. At other temperatures a helium-gas flow system was utilized with stabilization provided by feedback from a temperature sensor mounted on the sample to a heating element in the gas stream. When using the latter system the measurement of temperature was obtained from the resonant frequency of the F^{19} nuclei *not* associated with the impurity. Comparison of this resonance with the resonance in pure MnF_2 in the liquid-hydrogen temperature region showed them to be identical thus enabling us to use this method for temperature determination.

In contrast with the ferromagnet there is neither appreciable wall motion nor domain rotation in an antiferromagnet in response to an rf magnetic field. Hence the enhancement of the rf field experienced by nuclei in ferromagnets that are hyperfine coupled to the electronic spins is almost entirely absent in the antiferromagnet. Considerations then of the optimum rf field strength in a pulsed experiment in an antiferromagnet are similar to those for nuclei in any nonmagnetic medium. In the impurity-doped samples linewidths of the order of 100 G were encountered. To produce a 180° pulse in which most of the spins within the inhomogeneously broadened line were flipped required pulse widths as short as 2 μsec and rf field strengths as large as 100 G.

T_2 was measured using a conventional 90°–180° pulse sequence. In our samples the decays of the echo en-

[8] Model PH20K manufactured by Applied Microwave Laboratory, Inc., Andover, Mass.
[9] Model WA-600E manufactured by Arenberg Ultrasonic Laboratory, Inc., Boston, Mass.
[10] Model CW-1 manufactured by Princeton Applied Research Corp., Princeton, N. J.

velope were of the form

$$M(2\tau)=M(0)e^{-2\tau/T_2}. \quad (2)$$

The determining factor in how high in temperature we could make transient measurements was the rapid decrease of T_2 with T above 20°K caused by spin-lattice relaxation.

The position and profile of a given resonance was obtained in the following manner. Assume, for the moment, the F^{19} hyperfine field is parallel to the c axis. Then an external magnetic field, applied parallel to the c axis, will add to the hyperfine field at one (see Fig. 2) and subtract from the field at the other of the two inequivalent sites, giving two branches to each resonance. In this configuration ($\mathbf{H}_0 \| c$ axis) it is possible to fix the spin-echo spectrometer frequency and scan the external field to search for resonances in the manner shown in Fig. 3. This is far simpler than varying the frequency and holding the field fixed, as then one must ensure that the receiver, transmitter, and tuned resonance circuit frequencies track accurately. The results obtained in a particular fixed-frequency scan for MnF^{19}_2:Zn are shown in Fig. 4, where the ordinate is spin-echo amplitude for $2\tau \sim 30$ μsec and the abscissa is the external field. As 2τ was *not* much smaller than T_2, variations of T_2 from line to line and within a single line distort the line shapes and their relative amplitudes. However, by measuring T_2 for the various resonances the relative intensities of these resonances at $2\tau=0$ may be determined. These intensities provide a reasonably direct measure of the impurity concentrations while avoiding some of the pitfalls common with chemical analysis. From a set of field scans, each at a different frequency, we extract the desired, extrapolated zero-field resonant frequencies. It is here that care must be taken to correct for any sample misorientation and to properly take into account the finite parallel susceptibility at elevated temperatures.

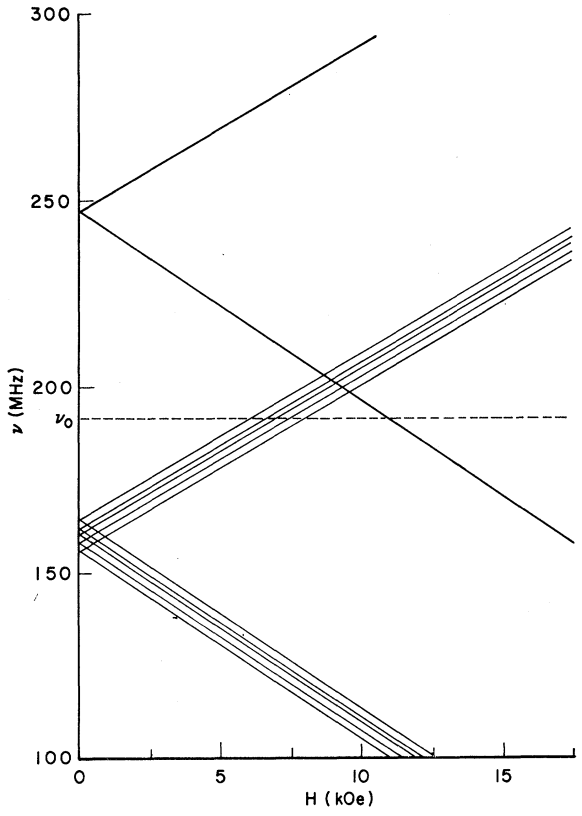

FIG. 3. A plot of frequency versus field applied parallel to the c axis for the F^{19} resonances that were observed in MnF_2:Zn at 4.2°K. The spin-echo experiments were performed at a fixed frequency ν_0 and the resonances observed by varying the field as shown.

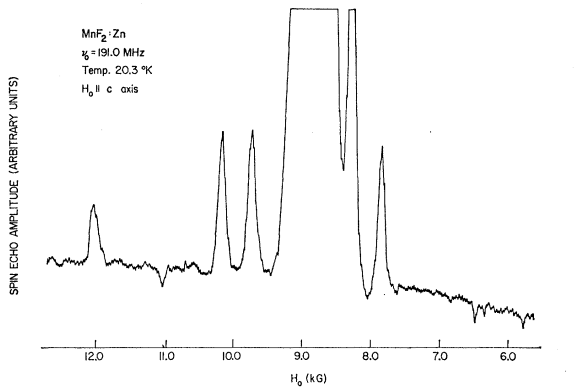

FIG. 4. The results of a typical field scan for MnF_2:Zn. Since it is the spin-echo amplitude that is observed, variations in T_2 from line to line, and even within a line, tend to distort relative intensities and line shapes. The flat top on the main line and one satellite line results from saturation of the detection system.

T_1 is measured by heating the nuclear spin system with a saturating comb and monitoring the return of $\langle M_z \rangle$ to equilibrium using a 90°–180° double pulse. The recovery of the magnetization very closely follows the form

$$M(t)=M(\infty)[1-e^{-t/T_1}]. \quad (3)$$

III. IMPURITY-ASSOCIATED RESONANCE LINES—POSITIONS AND WIDTHS

A. Positions of Resonances

It was pointed out in Sec. I that one of the more obvious effects of impurities is to produce a number of new F^{19} resonances. In order to examine the origin and properties of such resonances, we briefly review the origin and properties of the F^{19} resonance in pure MnF_2. Contributions to the internal magnetic field at the nucleus may be thought of as arising from two different interactions; the transferred hyperfine interaction which couples each F^{19} nucleus to the three neighboring Mn spins (see Fig. 2) and the dipolar interaction with all of the remaining Mn spins in the crystal. This leads to a

F^{19} nuclear Hamiltonian for the kth site of the form[11]

$$\mathcal{H}_n{}^k = -\gamma h \mathbf{I}_k \cdot \mathbf{H}_0 + \sum_j \mathbf{I}_k \cdot \mathbf{A}_{kj} \cdot \mathbf{S}_j + \sum_j \gamma h \beta \mathbf{I}_k \cdot \mathbf{g} \cdot \mathbf{S}_i \frac{(1-3\cos^2\theta_{ik})}{r_{ik}{}^3} + \mathcal{H}_{I,I}, \quad (4)$$

where the last term represents the nuclear spin-spin interactions. While there are off-diagonal components of the hyperfine and **g** tensors, the particular symmetry of the MnF_2 lattice results in a *time-average* cancellation of the off-diagonal terms. This results in the internal magnetic field being aligned parallel to the c axis and in the F^{19} resonant frequency, with the applied magnetic field $H_0 \| c$, being

$$\nu^{19} = A_z{}^{\mathrm{I}}\langle S_z{}^{\mathrm{I}}\rangle + A_z{}^{\mathrm{I}'}\langle S_z{}^{\mathrm{I}'}\rangle - A_z{}^{\mathrm{II}}\langle S_z{}^{\mathrm{II}}\rangle + \sum_{i\neq \mathrm{I},\mathrm{I}',\mathrm{II}} d_i \langle S_z{}^i\rangle \pm \gamma^{19} H_0. \quad (5)$$

The A's are the transferred hyperfine coupling constants along directions r^{I}, $r^{\mathrm{I}'}$, and r^{II} identified in Fig. 2 and d_i is the z component per spin of the dipolar field produced by Mn spins at sites other than the three neighboring sites. A given F^{19} nucleus is strongly influenced by the three neighboring magnetic sites through the transferred hyperfine interaction and to a lesser extent by the more distant sites through the dipolar interaction.

We are now in a position to explain the existence of the impurity-associated resonances. In the low-concentration limit where one need not worry about pairs, two types of impurity-induced frequency shifts may be distinguished: (i) the shift caused by a changed transferred hyperfine field when the impurity occupies one of the three neighboring magnetic sites to a given fluorine. Such shifts are illustrated in Fig. 5 for a nonmagnetic impurity and are on the order of 25 kG. For magnetic impurities one expects shifts $\lesssim$25 kG. (ii) The shift caused by changes in the dipolar field when the impurity occupies any site other than the three nn ones: Four such shifted resonances are illustrated in Fig. 5 for a nonmagnetic impurity. The maximum shifts in this case are of the order of 1 kG.

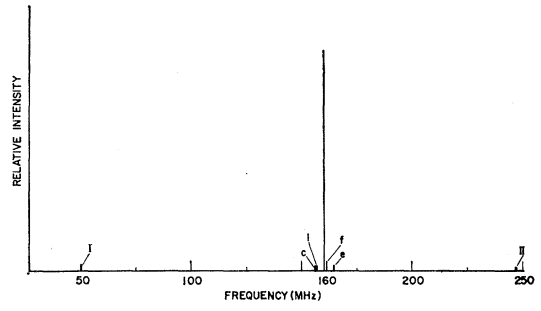

FIG. 5. A schematic representation of the F^{19} resonances in MnF_2:Zn with no applied field. The four resonances near the main line are "dipolar" lines with the resonances of larger frequency shifts being "hyperfine" lines. The resonance intensities are scaled to the main line and are identified with the corresponding F^- sites.

[11] R. G. Shulman and V. Jaccarino, Phys. Rev. **108**, 1219 (1957).

It is evident from the above that the different impurity-associated resonances sample distinct regions in the vicinity of the impurity. In order to see this clearly, we will now consider a more detailed identification of the various lines. From Eq. (5) it is easy to show that the frequency for resonance of the impurity-associated F^{19} nuclei of type (ii) considered above may be expressed as

$$\nu_i = \sum_k^{\mathrm{I},\mathrm{I}',\mathrm{II}} A_z{}^k(\mathrm{Mn})\langle S_z\rangle^k + \sum_{j\neq k} d^j \langle S_z{}^{\mathrm{Mn}}\rangle^j - \frac{\gamma^{19}\beta}{r_i{}^3}(3\cos^2\theta_i - 1)[g(\mathrm{Mn})\langle S_z{}^{\mathrm{Mn}}\rangle - g(\mathrm{imp})\langle S_z{}^{\mathrm{imp}}\rangle], \quad (6)$$

where r_i and θ_i are the coordinates with respect to the impurity of the ith F^{19} nucleus which is *not* a nn to the impurity. The last term is the correction of the dipolar field at the ith site arising from replacement of the Mn spin by the impurity spin. Therefore, the frequency *shifts* with respect to the main resonance are

$$\Delta\nu_i = \frac{-\gamma^{19}\beta}{r_i{}^3}(3\cos^2\theta_i - 1) \times [g(\mathrm{Mn})\langle S_z{}^{\mathrm{Mn}}\rangle - g(\mathrm{imp})\langle S_z{}^{\mathrm{imp}}\rangle]. \quad (7)$$

The various F^{19} sites relative to a single impurity which may have their resonant frequencies shifted significantly are shown in Fig. 6. The sites labeled c, d, e, and f are the ones responsible for the "dipolar" lines. At the concentrations we have examined, only these sites produce shifts that sufficiently displace the individual resonances so that they are separate and distinct from the main resonance. The shifts $\Delta\nu_i$ for these sites have been calculated for the various impurities and are compared with the observed spectra in Fig. 7. The spectra are arranged in order of decreasing difference between the impurity and Mn electronic magnetic moments. It is to be noted, first, that $\Delta\nu_i \propto (\mu_{\mathrm{imp}} - \mu_{\mathrm{Mn}})$. Second, it is apparent that, although in a number of cases a resonance appears where we have calculated one should be, numerous discrepancies exist. Hence, position and relative intensity are insufficient to uniquely identify all of the resonances. However, an unambiguous identification can be obtained but requires an examination of the temperature dependence of these resonances (see Sec. IV). Once having been identified, it is found that the calculated position for sites c and e are quite accurate but systematic differences exist for sites l and f. These differences are attributable to strain effects caused by the presence of the impurity and are examined in detail in the Appendix.

The clear identification of resonances associated with the nearest-neighbor sites to an impurity, type (i), is much easier. In general, the frequency shifts are much larger than the dipolar shifts and only two distinct sites exist—labeled I and II in Fig. 6—with the sites labeled I contributing a resonance intensity double that of II. If the frequency shifts are sizable (i.e., larger than the dipolar shifts) identification is almost trivial. With no externally applied field the frequencies for resonance of these sites are

$$\nu^{\mathrm{I}}=A_z{}^{\mathrm{I}}(\mathrm{Mn})\langle S_z{}^{\mathrm{Mn}}\rangle_{\mathrm{I}}+A_z{}^{\mathrm{I}}(\mathrm{imp})\langle S_z{}^{\mathrm{imp}}\rangle - A_z{}^{\mathrm{II}}(\mathrm{Mn})\langle S_z{}^{\mathrm{Mn}}\rangle_{\mathrm{II}}+\sum_{i\neq \mathrm{I},\mathrm{I}',\mathrm{II}} d_i\langle S_z{}^i\rangle \quad (8a)$$

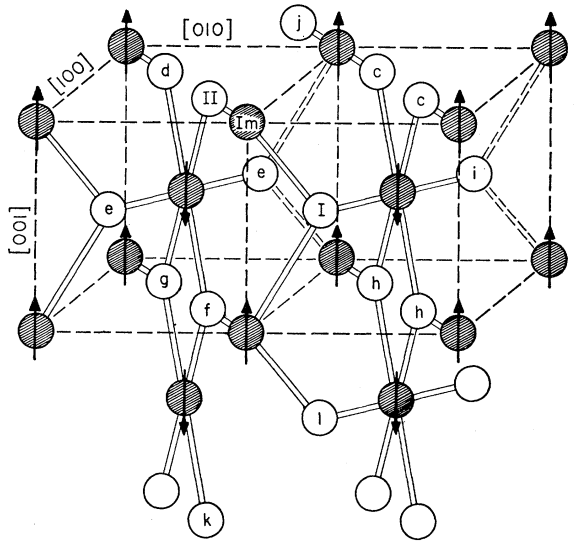

FIG. 6. A more extensive representation of the crystal and magnetic structure of MnF_2 wherein the various F^- sites (clear balls) are identified relative to an impurity (Im). The shaded balls are the magnetic sites with the arrows again showing the direction of electronic spin magnetization in the ordered state.

and

$$\nu^{\mathrm{II}}=2A_z{}^{\mathrm{I}}(\mathrm{Mn})\langle S_z{}^{\mathrm{Mn}}\rangle_{\mathrm{I}}-A_z{}^{\mathrm{II}}(\mathrm{imp})\langle S_z{}^{\mathrm{imp}}\rangle + \sum_{i\neq \mathrm{I},\mathrm{I}',\mathrm{II}} d_i\langle S_z{}^i\rangle. \quad (8b)$$

As a first approximation in calculating the resonance shifts, we may assume no impurity-induced strain effects are present and use for the Mn hyperfine coupling constants those determined in pure $MnF^{19}{}_2$ and for the impurity (X) those obtained from F^{19} NMR in pure XF_2. In all cases we neglect zero-point effects completely. Frequencies calculated in this approximation, as well as those calculated for the "dipolar" lines, are compared to the observed resonances (of course, assuming proper identification) in Table I. Although these calculated frequencies qualitatively indicate where one would expect a particular resonance,

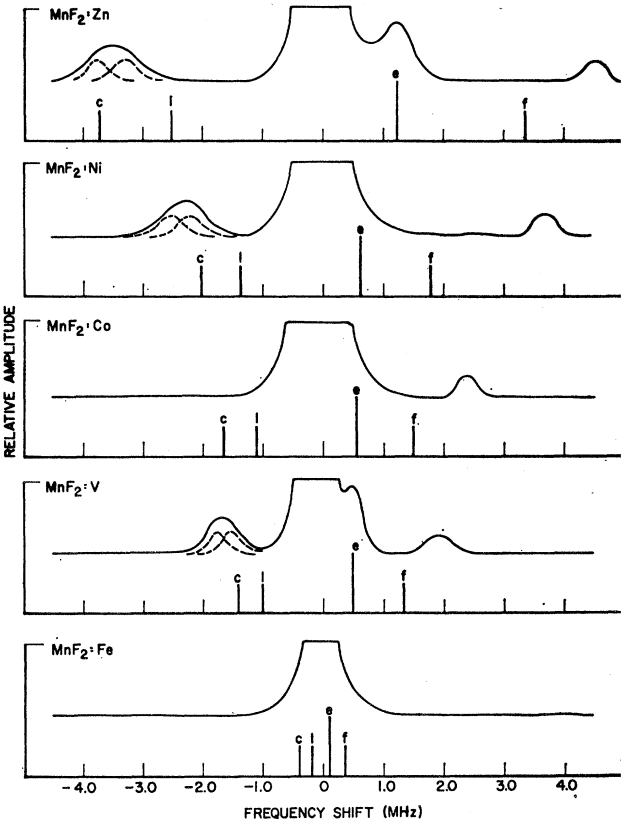

FIG. 7. The position and amplitudes of the observed "dipolar" lines at 0°K are compared with the calculated positions and amplitudes *neglecting strain effects*. The frequency shift is measured with respect to the main F^{19} resonance and the spectra are arranged in order of decreasing difference between the impurity and Mn electronic magnetic moments. The lines which are shown as the sum of two individual lines are actually resolved at higher temperatures because the temperature dependences of the two lines differ.

TABLE I. The observed zero-field frequencies of the impurity-associated resonances at 4.2°K are compared with the calculated ones, neglecting strain-induced effects. The calculated value marked by a † takes into account the canting of the F^{19} quantization direction due to the noncancellation of $A_{yz}{}^{\mathrm{I}'}$ and $A_{yz}{}^{\mathrm{I}}$. The uncertainty in the value of the Co^{2+} spin in $Co:MnF_2$ makes it difficult to estimate the frequencies of the resonances I and II (indicated as *). However, we have calculated the pure $CoF_2{}^{19}$ frequency from the impurity hyperfine coupling constants to be 161 MHz compared with the observed value of 143.88 MHz.

Sample	Site (MHz)	I	II	c	e	f	l
V:Mn F_2	Obs.	···	265.70	158.23	160.48	161.88	158.43
	Calc.	···	···	158.60	160.50	161.35	159.00
Fe:Mn F_2	Obs.	173.42	155.36	···	···	···	···
	Calc.	177	160	159.61	160.11	160.34	159.81
Co:Mn F_2	Obs.	140.56	198.17	···	···	162.40	···
	Calc.	*	*	158.37	160.55	161.48	158.89
Ni:Mn F_2	Obs.	161.40	178.22	157.80	···	163.68	157.50
	Calc.	169	169	158.02	160.67	161.80	158.65
Zn:Mn F_2	Obs.	···	247.12	156.25	161.25	164.55	156.65
	Calc.	50†	257	156.29	161.26	163.37	157.48

again there are significant differences. These discrepancies we attribute to impurity-induced strains which are explored in detail in the Appendix.

B. Resonance Broadening (Inhomogeneous)

Another quite obvious effect of impurities, aside from the generation of new resonances, is the dramatic increase in the broadening of all resonances, old and new, as the impurity concentration increases. For example, in nominally 1% Zn-doped MnF_2 the linewidths are of the order of $\sim$100 G compared to $\sim$5 G for pure $MnF^{19}{}_2$. The absence of a free-induction decay signal when performing a transient experiment and the long T_2's observed indicate that the impurity-related broadening is static in nature. The broadening is caused by spatial fluctuations of the local dipolar field when Mn moments are randomly replaced by the impurity moments. Of course, for the F^{19} nuclei adjacent to an impurity only distinct lines result. However, the dipolar contribution to the local field from more distant, but numerous, impurities will result in an overlapping array of very closely spaced resonances whose envelope is the broadened line. Applying Van Vleck's moment method[12] we calculate the linewidth as a function of impurity concentration. The second and fourth moments, respectively, are given by

$$M_2'=\sum_i{}' (\Delta\nu_i)^2 \tag{9a}$$

and

$$M_4'=\sum_i{}'(\Delta\nu_i)^4, \tag{9b}$$

where the prime on $\sum$ denotes the summation is restricted to impurity sites and $\Delta\nu_i$ is defined by Eq. (7). For a completely random distribution of impurities the restricted sums may be taken as the concentration c times the unrestricted sums[13]:

$$M_2'=c\sum_i(\Delta\nu_i)^2\equiv cM_2,$$

$$M_4'=c\sum_j(\Delta\nu_i)^4\equiv cM_4.$$

Since for small concentrations ($\lesssim$0.01) the ratio $M_4'/(M_2')^2\gg 3$, the inhomogeneously broadened line profile will tend more towards being Lorentzian in shape. A useful approximation in this instance is the truncated Lorentzian model, as it is characterized by only two parameters and we have but two moments. For this model the linewidth (full width at half-maximum) is

$$\delta=\frac{\pi}{\sqrt{3}}\frac{(M_2')^{3/2}}{(M_4')^{1/2}}=\frac{\pi}{\sqrt{3}}\frac{(M_2)^{3/2}}{(M_4)^{1/2}}, \tag{10}$$

[12] J. H. Van Vleck, Phys. Rev. **74**, 1168 (1948).
[13] A. Abragam, *The Principles of Nuclear Magnetism* (Oxford University Press, New York, 1961).

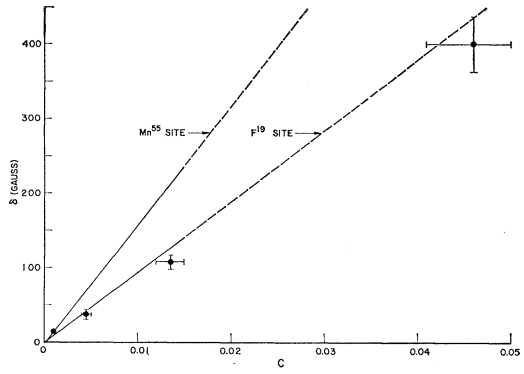

FIG. 8. The inhomogeneous linewidth as a function of impurity concentration C in MnF_2:Zn. The experimental data points are for F^{19} nuclei and agree with the linewidth calculated in the low-concentration limit. The calculated inhomogeneous linewidth for the Mn^{55} resonance is also shown.

from which we see that for low impurity concentrations the linewidth is proportional to the concentration. We have explicitly calculated the linewidth of the main F^{19} resonance for $Zn_cMn_{(1-c)}F_2$ by performing the moment sums numerically over the MnF_2 lattice. Those sites that would produce a separate resonance were excluded. Experiment and theory, as seen in Fig. 8, are in excellent agreement showing that strains generated by the impurities do not contribute significantly to the line broadening.

Figure 8 also shows the broadening expected at the Mn^{55} nucleus in the same sample. Because the Mn^{55}-Mn^{55} Suhl-Nakamura (SN) interaction is so large, a concentration $c\gtrsim 3\%$ Zn is required to produce an inhomogeneous (static) contribution to the linewidth comparable to the homogeneous linewidth observed in pure MnF_2.[14] This would account for the fact that neither inhomogeneous broadening of the resonance nor evidence of spin echoes were observed in the Mn^{55} NMR studies made in these impurity-doped samples.[14]

C. Resonance Broadening (Homogeneous)

T_2 has been measured for a variety of F^{19} resonances in the impure crystal. Understanding the results obtained necessitates first understanding the origin of T_2 in pure MnF_2. In a relatively perfect crystal, in which no echoes were observable without deliberately superimposing an inhomogeneous magnetic field, the decay of the echo envelope was exponential and a value of $T_2=29\pm1$ μsec was found.[15] The inferred Lorentzian shape to this homogeneously broadened line suggests that an "exchangelike" narrowing of the spin-spin interactions must be present. This arises from the rapid modulation of the F^{19}-Mn^{55} dipolar interaction by the large Mn^{55}-Mn^{55} SN coupling. A detailed analysis of

[14] H. Yasuoka, T. Ngwe, V. Jaccarino, and H. J. Guggenheim, Phys. Rev. **177**, 667 (1969).
[15] N. Kaplan, P. Pincus, and V. Jaccarino, J. Appl. Phys. **37**, 1239 (1966).

this problem along with expressions for the relevant second and fourth moments may be found in Ref. 16. Evaluation of the expressions for the second and fourth moments yields the following values: $M_2^{F-F}=3.35\times10^{-45}$ erg^2; $M_2^{F-Mn}=3.00\times10^{45}$ erg^2; and $M_4=2.20\times10^{-87}$ erg^2. Again, because $M_4/(M_2^2)\gg3$, we use the truncated Lorentzian model to calculate δ. As

$$\frac{1}{T_2}=\frac{\delta}{2}=\frac{\pi}{2\sqrt{3}}\frac{(M_2^{F-F}+M_2^{Mn-F})^{3/2}}{M_4^{1/2}}, \quad (11)$$

we obtain a value of $\delta=0.74$ G or a $T_2=107$ μsec. We feel the discrepancy between theory and experiment $\delta^{expt}/\delta^{theor}\sim3.6$, results from the inadequacy of the truncated Lorentzian model. It has been shown[17] that, in those cases where strong exchange narrowing is present and all of the pertinent parameter are accurately known, the truncated Lorentzian model underestimates the linewidth by a factor of 2–3.

While the Mn^{55}-F^{19} dipolar coupling appears necessary to explain the Lorentzian nature of the dynamic line shape, it would be reassuring to see a more direct indication of its importance. This is made possible by introducing a number of impurities sufficient to completely detune the F^{19}-F^{19} interaction while leaving the $I_z^{Mn}I_z^F$ coupling and M_4 essentially unchanged. In this case, we would expect T_2, as a function of impurity concentration c, to asymptotically approach a constant value. Of course, the exact dependence of T_2 on c and the final value of T_2 in the limit of complete F^{19}-F^{19} detuning depends on the model used. Even though a cutoff Lorentzian line profile has proven inadequate for calculating T_2 in pure MnF^{19}_2, it gives us an indication what to expect in the limits of complete F^{19}-F^{19} detuning. In this limit the model yields

$$T_2=T_2^{pure}\left(1+\frac{M_2^{F-F}}{M_2^{Mn-F}}\right)^{3/2}, \quad (12)$$

where the moments are those calculated for pure MnF_2. Figure 9 shows the variation of T_2 at the center of the main F^{19} resonance in MnF_2:Zn as a function of impurity concentration c. Notice that T_2 does approach

TABLE II. The values of T_2 for resonances of F^{19} nuclei which have various impurities at type I and II neighboring sites. The symbols * and † mean the following: *, signal too weak to obtain a meaningful result; †, these values are suspect as other measurements indicate the presence of paramagneticlike impurities.

T_2(μsec) Site	Impurity V	Fe	Co	Ni	Zn
I	···	30†	64	···	···
II	*	112†	162	200	166

[16] D. Hone, V. Jaccarino, Tin Ngwe, and P. Pincus, Phys. Rev. **184**, 371 (1969).

[17] J. E. Gulley, B. G. Silbernagel, and V. Jaccarino, J. Appl. Phys. **40**, 1318 (1969).

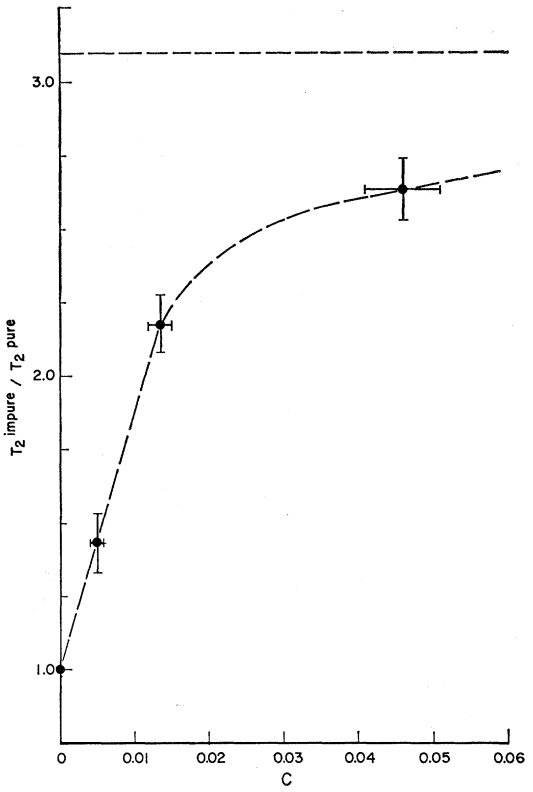

FIG. 9. The ratio of T_2 at the center of the main F^{19} resonance in MnF_2:Zn to T_2 in pure MnF_2 as a function of impurity concentration. The horizontal dashed line at 3.1 is the limiting ratio expected for complete decoupling of the F^{19}-F^{19} dipolar interaction due to the inhomogeneous broadening caused by the impurity.

the expected value for complete F^{19}-F^{19} detuning, providing further evidence for the importance of the Mn^{55}-F^{19} dipolar coupling in MnF_2.

We have also measured T_2 for various impurity-associated resonances in nominally 1% impurity-doped samples. As all of the dipolar lines overlapped the main line to some extent, it is not surprising that their T_2's are very similar to each other and only differ slightly from the T_2 of the main line. The overlap makes any detailed interpretation difficult. However, the resonances associated with the type I and II sites are well separated from the main resonance. Table II gives the T_2's for the type I and II resonances for various impurities. The results in MnF_2:Fe are somewhat suspect because the impurity-associated resonance intensities, linewidths, and T_1's indicate that "paramagnetic" impurities are present. We can explain the results in Table II by appropriate modification of the moments calculated for the F^{19} resonance in pure MnF_2. Consider first, the change in M_2^{Mn-F} that results from impurities for the type I and type II F^{19} sites. The difference in the angular factors for those sites and the fact that one of the neighboring Mn^{55} dipoles has been removed results in values for the two moments of $M_2^{Mn-F}(II)\sim0.61$ M_2^{Mn-F} and $M_2^{Mn-F}(I)\sim0.74$ M_2^{Mn-F}, where M_2^{Mn-F}

is the pure MnF_2 moment. The corresponding changes in M_2^{F-F} at the two sites adjacent to the impurity are obtained as follows: For appreciable inhomogeneous broadening only "like" F^{19} nuclei contribute to the T_2's. There are but two equivalent type II F^- ions for an isolated impurity and these are separated by a large distance (4.3 Å). The interaction between these two is so small that it is reasonable to take $M_2^{F-F}(II)\approx 0$. However, for each impurity there are four equivalent type I site nuclei which strongly interact with each other. Assuming these alone contribute to $M_2^{F-F}(I)$, we find, relative to the pure crystal value, that $M_2^{F-F}(I) = 0.57\ M_2^{F-F}$. In the first approximation M_4 is unmodified from the pure MnF_2 value because the Mn^{55}-Mn^{55} SN interaction, which dominates M_4, is unaffected by the presence of impurities at these low concentrations.

Again using the truncated Lorentzian model, we may calculate values for the T_2's of the two sites using the relation

$$(T_2^{I,II})^{-1} = \frac{\pi}{2\sqrt{3}} \frac{[M_2^{F-F}(I,II)+M_2^{M-F}(I,II)]^{3/2}}{M_4^{1/2}}, \quad (13)$$

for which we find $T_2^I = 215\ \mu$sec and $T_2^{II} = 696\ \mu$sec.

However, recalling the discrepancies that were observed between theory and experiment for pure MnF^{19}_2, we adjust the above results by the same scale factor required to obtain agreement for pure MnF_2 (i.e., $\delta^{expt}/\delta^{theor} = 3$). In this manner, we find values of $T_2^I(adj) = 58\ \mu$sec and $T_2^{II}(adj) = 189\ \mu$sec which are in surprisingly good agreement with experiment considering the approximate nature of the model.

D. Effects of Larger Concentrations of Impurities

So far we have been concerned with the low-concentration limit and have only considered resonances associated with single impurities. We will now digress somewhat to show what may be learned from studies of higher impurity concentrations and mixed crystals. We have already seen that large inhomogeneous linewidths are caused by variations in the electronic dipolar field due to the random distribution of impurities. Obviously this kind of line broadening is proportional to the *difference* between the host and the impurity moments and increases with impurity concentration. Clearly then, for excessive line broadening not to obscure the resonances, either the impurity concentration must be relatively low ($<5\%$) or one must look at systems where host and impurity moments are rather similar. (It does not matter how different are the spins or the exchange couplings.)

As an example of the moderate impurity concentration case, we have searched for F^{19} resonances in 5% MnF_2:Zn arising from *two* of the neighboring magnetic ions being replaced by Zn^{2+} ions. The two possibilities are the I–I resonance, whose frequency is $\nu^{I-I} \sim A_{zz}^{II}\langle S_z^{II}\rangle$, and the I–II resonance whose frequency is $\nu^{I-II} \sim [(A_{zz}^I)^2+(A_{yz}^I)^2]^{1/2}\langle S_z^I\rangle$ (see Fig. 2). Note that because of the transverse component of the hyperfine field for the I–II resonance, the direction of quantization for this F^{19} nucleus will be canted at an angle $\varphi = \tan^{-1}(A_{yz}^I/A_{zz}^I)$ with respect to the c axis. Neglecting strain effects the following values for the zero-field resonant frequencies are predicted: $\nu_0^{I-I} \simeq 107.5$ MHz; $\nu_0^{I-II} \simeq 127.0$ MHz.

Only a single resonance in this vicinity was observed at a field of 16 kG. We tentatively identify this resonance as ν^{I-II} which, when extrapolated to zero field, yields $\nu_0^{I-II} \simeq 119$ MHz. We attribute the small difference between theory and experiment to strain effects, since it is of the same sign and magnitude as was observed for the Zn-II resonance. We believe it to be unlikely that the observed resonance is ν^{I-I}, since strains tend to reduce rather than increase the resonance frequency.

The question naturally arises as to why we were unable to observe ν^{I-I}. A combination of factors is probably involved. First, all of the lines are very wide ($\sim$400 G) making them difficult to see and for a random distribution of Zn^{2+} ions the I–I resonance should be a factor of 2 weaker than the I–II. Second, the ratio of intensities of the I–II and II (single) impurity lines is five times smaller than expected for a completely random distribution. This tendency toward anticlustering for the Zn^{2+} ions in the solvent lattice may be stronger for the I–I configuration than the I–II. Finally, it is possible that the T_1 associated with the resonance ν_{I-I} is so large that with the scanning technique used, we would not have observed the line. Larger values of T_1 are expected because simple two-magnon hyperfine coupled relaxation processes are no longer allowed. This point is discussed in Sec. IV in greater detail. The two-magnon process responsible for T_1 in pure MnF_2 requires off-diagonal elements in the hyperfine coupling tensor. The only off-diagonal elements come from the I and I' sites. Since the I–I resonance arises from both of these sites being occupied by nonmagnetic Zn ions, no simple hyperfine coupled two-magnon scattering is possible in this instance.

Additional structure was noted on the single-impurity spectra. For example, "shoulders" were observed on the Zn-II resonance, but the extreme line broadening made further resolution impossible. We believe this "structure" to be dipolar satellites of the Zn-II resonance caused by a second Zn^{2+} ion.

As an example of a high concentration system in which the host-impurity moment difference Δ is relatively small, we have studied $Mn_{0.5}Fe_{0.5}F_2$. Despite the fact that Δ is only of order μ_B, instead of $5\mu_B$ as in the Zn-doped crystals considered above, the larger value of c results in linewidths of 500–1000 G for the various F^{19} resonances. The large linewidths obscure all dipolar lines. Hence, we would expect to see but six hyperfine lines corresponding to the six possible configurations

TABLE III. The F^{19} resonances observed in $Mn_{0.5}Fe_{0.5}F_2$. The configuration is the arrangement of the three neighboring magnetic ions. The intensities were calculated for a random distribution and the frequencies were calculated for zero temperature using the single-impurity coupling constants but allowing for changes in the local dipolar fields. Because of the severe inhomogeneous broadening no "dipolar" lines were observed.

Configuration	Calc. intensity	Obs. intensity	Calc. freq.	Obs. freq.
$Mn^{I}Mn^{I}Mn^{II}$	0.125	0.08	160	163
$Mn^{I}Mn^{I}Fe^{II}$	0.125	0.08	155	157
$Mn^{I}Fe^{I}Mn^{II}$	0.250	0.37	173	176
$Mn^{I}Fe^{I}Fe^{II}$	0.250	0.33	169	167
$Fe^{I}Fe^{I}Mn^{II}$	0.125	0.08	187	192
$Fe^{I}Fe^{I}Fe^{II}$	0.125	0.08	183	180

obtained by permitting either Mn or Fe ions in each of the three neighboring positions to a given F^- ion. Table III gives the estimated frequencies for these various configurations. Six resonances are observed and have been associated with the six configurations. While the frequencies are quite close and the relative intensities are not in disagreement, strain-induced frequency shifts may result in improper identification.

Certain features of Table III are of particular interest. The configurations with the same ions in both type I sites have relative intensities weaker than calculated on the basis of a random distribution. This indicates again, as in the 5% MnF_2:Zn sample, that a stronger tendency exists for anticlustering in the I-I configuration than in the I-II. Another peculiarity that is apparent in the tabulated data is that the configurations with two or three Mn^{2+} ions have observed frequencies higher than are calculated. We believe this to be a consequence of the MnF_2 lattice being larger than the FeF_2 lattice. It follows, that in the mixed crystal the F^- ions are closer to the Mn^{2+} ions than in pure MnF_2. With decreased Mn^{++}-F^- separations the transferred hyperfine coupling constants increase (and hence the frequencies) for the Mn^{2+}-dominated configurations. Conversely, for the Fe^{2+}-dominated configurations one would expect the observed frequencies to be lower than those calculated. The discrepancy for the $Fe^{I}Fe^{I}Mn^{II}$ configuration may be attributed to uncertainty about the local environment of Fe impurities in MnF_2 as single-impurity coupling constants were used to calculate the frequencies.

It thus appears that NMR in mixed crystals is capable of giving some information about the distribution of ions and providing a probe which enables one to examine regions rich in one type of ion or the other.

IV. IMPURITY THERMODYNAMICS

We have shown in Sec. III that the various new F^{19} resonances that result from an impurity substitutionally replacing a Mn^{2+} ion in MnF_2 are directly correlated with certain changes in the hyperfine or dipolar interactions in the vicinity of the impurity. Because of the one-to-one correspondence between the particular resonance frequency and the position of the F^- ion relative to the impurity, the resonance spectra offer the possibility of probing the local magnetic disturbance caused by the introduction of the impurity. The features most susceptible to direct analysis using our resonance techniques are the thermodynamics associated with the creation of impurity modes. The particular thermodynamic properties we will consider here are the temperature dependencies of the magnetization $[M_i(T)]$, the parallel susceptibility $\chi_i''(T)$ and the nuclear spin-lattice relaxation rate $(1/T_1)_j$. Here i labels either the impurity or any one of its Mn^{2+} neighbors, nearest or otherwise, and j the F^{19} nuclear site which is at position $\mathbf{r}_{kj}$ from the impurity at site k.

A. Experimental Results

1. Derived Values of $M_i(T)$

The temperature dependencies of the various impurity-associated resonances are listed in Table IV. Not all of the resonances and their temperature dependencies are available for a variety of reasons most of which were given in the previous section. This presents some difficulties in the interpretation of the derived quantities in these instances as does our limited accuracy resulting from the instability of our sample temperatures above 20°K. All of this notwithstanding, we have been able to derive values of $M_i(T)$ for the impurity and its nearest- and next-nearest neighbors in almost all of the cases of interest.

Remembering that each F^{19} nucleus is hyperfine coupled to its three nn ions, we note first that the temperature dependence of any given resonance must reflect a suitably weighted average of the temperature dependencies of the hyperfine fields of those same neighbors. The three neighboring sites for each of the six impurity-associated resonances are shown in Fig. 10. We have made the following simplifying assumption: *Any Mn site that is neither a nn nor nnn to an impurity is taken to have a temperature dependence to its magnetization which is identical to that of the host.* This assumed localization of the variation of the magnetization from that of the host is intimately related to the nature of the impurity magnon modes. Both for modes that are either high or low in energy with respect to the region of high state density in the host we would expect to have strongly localized states. In addition, at temperatures low compared to the ordering temperature, localization will be prevalent even if the above more stringent conditions are not satisfied.[18] Experimentally we find *no* evidence to contradict our assumption.

A second point to be made concerning the classification of sites shown in Fig. 10 is that we have made a distinction between the two nnn sites (labeled x and y) because their local site symmetries differ. The tempera-

[18] D. Hone and L. R. Walker (private communication).

TABLE IV. A detailed summary of the temperature dependences of all the impurity-associated F^{19} NMR frequencies in the MnF_2:X systems. For the "dipolar" lines only the deviations from the main F^{19} resonant frequency are given.

	Zn					Ni				Co		Fe		V				
Temp. (°K)	ν(II)	$\Delta\nu(c)$	$\Delta\nu(e)$	$\Delta\nu(f)$	$\Delta\nu(l)$	ν(II)	$\Delta\nu(c)$	$\Delta\nu(f)$	$\Delta\nu(l)$	ν(I)	ν(II)	ν(I)	ν(II)	ν(II)	$\Delta\nu(c)$	$\Delta\nu(e)$	$\Delta\nu(f)$	$\Delta\nu(l)$
4.2	247.12	−3.72	+1.28	+4.58	−3.32	178.36	−2.17	+3.71	−2.47	140.56	198.17	173.42	155.36	265.70	−1.74	+0.51	+1.92	−1.54
14.0	244.52	−4.35	+1.58	+4.32	−3.56	176.83	−2.17	+3.96	−2.62	139.93	196.50	173.04	154.15	259.65	−2.00	+0.60	+1.80	−1.60
15.0	243.93	−4.62	+1.64	+4.32	−3.71	176.40	−2.17	+4.01	−2.72	139.72	196.04	172.99	153.78		−2.00	+0.70	+1.75	−1.60
16.0	243.14	−4.82	+1.68	+4.15	−3.70	175.88	−2.17	+4.06	−2.77	139.47	195.53	172.89	153.45		−2.15	+0.73	+1.80	−1.60
17.0	242.38	−5.09	+1.75	+4.02	−3.73	175.35	−2.17	+4.08	−2.88	139.25	194.94	172.79	152.93		−2.15	+0.74	+1.80	−1.65
18.0	241.48	−5.24	+1.87	+4.05	−3.72	174.74	−2.12	+4.09	−2.97	139.04	194.23	172.56	152.47		−2.25	+0.76	+1.80	−1.70
19.0	240.50	−5.45	+1.97	+3.94	−3.77	174.10	−2.10	+4.16	−2.97	138.70	193.52	172.53	151.81		−2.40	+0.78	+1.80	−1.80
20.3	239.18	−5.83	+2.03	+3.73	−3.87	173.15	−2.07	+4.21	−3.10	138.35	192.51	172.30	150.88	254.34	−2.55	+0.80	+1.75	−1.90
20.8	238.26									137.96	191.73							
21.7	237.32																	
22.0						171.72		+4.31				172.04	149.01					
22.3															−2.90	+0.85	+1.70	−2.10
22.8										137.33	189.94							
23.1	235.80																	
24.0						169.95		+4.46										
24.6												171.17	146.66					
24.7										136.69	187.83				−3.30	+0.80	+1.50	−2.50
25.8	232.50																	
25.9						167.69		+4.61										
26.6										135.88	185.61							
27.0												170.54	144.25					
27.8	229.10																	
27.9						165.47		+4.76										
28.5										134.89	183.42							

ture dependencies of the various resonances and shifts, then, are

$$\nu^{\mathrm{I}}=A_i{}^{\mathrm{I}}S_i\sigma+A^{\mathrm{I}}S\sigma_{\mathrm{nn}}-A^{\mathrm{II}}S\sigma^x{}_{\mathrm{nnn}}+\gamma H_D\Sigma\,, \quad (14a)$$

$$\nu^{\mathrm{II}}=2A^{\mathrm{I}}S\sigma^y{}_{\mathrm{nnn}}-A_i{}^{\mathrm{II}}S_i\sigma+\gamma H_D\Sigma\,, \quad (14b)$$

$$\Delta\nu^{(c)}=2A^{\mathrm{I}}S(\sigma^x{}_{\mathrm{nnn}}-\Sigma)\,, \quad (14c)$$

$$\Delta\nu^{(l)}=A^{\mathrm{I}}S(\sigma_{\mathrm{nn}}-\Sigma)\,, \quad (14d)$$

$$\Delta\nu^{(f)}=A^{\mathrm{I}}S(\sigma^y{}_{\mathrm{nnn}}-\Sigma)-A^{\mathrm{II}}S(\sigma_{\mathrm{nn}}-\Sigma)\,, \quad (14e)$$

$$\Delta\nu^{(e)}=-A^{\mathrm{II}}S(\sigma^y{}_{\mathrm{nnn}}-\Sigma)\,, \quad (14f)$$

where the A's are the transferred hyperfine coupling constants with subscript i for the impurity, σ is the impurity magnetization, Σ is the host magnetization, and σ_{nn}, $\sigma^x{}_{\mathrm{nnn}}$, $\sigma^y{}_{\mathrm{nnn}}$ are the magnetizations of the Mn, nn, and nnn sites, respectively. The dipolar lines are measured with respect to their zero-temperature values [i.e., $\Delta\nu^{(c)}=\Delta\nu^{(c)}(T)-\Delta\nu^{(c)}(0)$] and have been diminished by the host magnetization. The reason for doing this is that it is experimentally more convenient to measure frequencies with respect to the main F^{19} resonance. We tacitly assume the hyperfine coupling constants to be temperature-independent and hence the temperature dependencies of the six resonances are only functions of the five reduced magnetizations.

In fact, what we want is the temperature dependence of each of the σ_i's in terms of the measured frequencies and shifts. To accomplish this we use the following procedure. As a first approximation, we assume the transferred hyperfine constant, associated with any of the two type of Mn-F couplings, are identical with their counterparts in pure MnF_2. From this we determine the two impurity transferred hyperfine coupling constants by a $T=0$°K measurement using Eqs. (14a) and (14b).

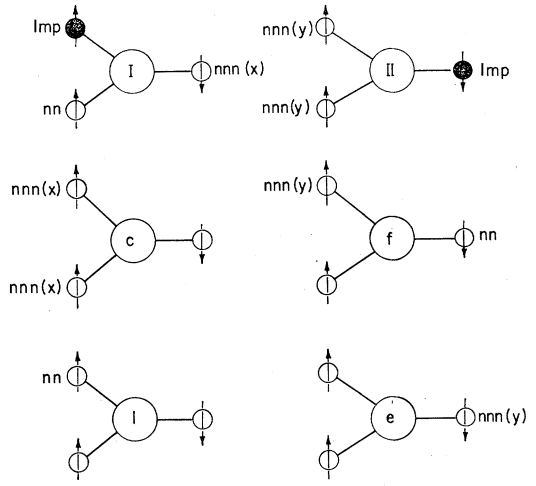

FIG. 10. The local environment of various F^- sites in the (110) plane showing their three nearest magnetic sites. Only the impurity, its nearest neighbor, and two types of next-nearest neighbor [nnn(x),nnn(y)] are distinguished from the rest of the crystal. Obviously because of the symmetry of the crystal, there are corresponding sites with all electronic spin directions reversed.

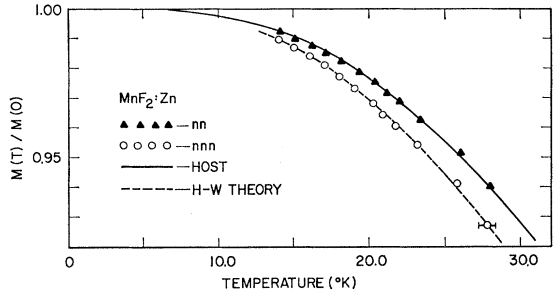

FIG. 11. The normalized experimental magnetizations for the nn and nnn Mn^{2+} sites to a Zn^{2+} impurity in MnF_2:Zn. These are compared with the host magnetization and the prediction of the Hone-Walker theory (Ref. 33) for the nnn magnetization.

With all of the constants "known" all of the magnetizations may be calculated, at each temperature, as if one has six equations and only four unknowns. The errors introduced by using the pure MnF_2 transferred hyperfine coupling constants are small providing the impurity coupling constants are comparable to the Mn coupling constants. For example, if $\sigma^y{}_{\mathrm{nnn}}$ is known from a measurement of $\Delta\nu^{(e)}$ and we determine σ from the II resonance, the error introduced by choosing the wrong Mn coupling constant is

$$\Delta\sigma^{\mathrm{II}}=(\sigma-\sigma^y{}_{\mathrm{nnn}})\frac{2\Delta A^{\mathrm{I}}S}{A_i{}^{\mathrm{II}}S_i}. \quad (15)$$

Since the change ΔA^{I} in A^{I} caused by strains is $\Delta A^{\mathrm{I}}\simeq 0.05A^{\mathrm{I}}$, we would find that σ_{nn} would be in error by $\Delta\sigma^{\mathrm{II}}\simeq 0.001$, assuming $A^{\mathrm{I}}\approx A^{\mathrm{II}}$. Because MnF_2 has the largest lattice constants of all the iron group fluorides, errors of this sort may be further reduced by assuming strain effects for all impurities are the same as those observed in Zn-doped MnF_2 where ΔA^{I} can be (and has been) measured.

As an example of the above analysis let us first consider MnF_2:Zn. The Zn^{2+} ion with a $3d^{10}$ closed-shell configuration is a spinless impurity (i.e., $\sigma\equiv 0$). Since all resonances except ν^{I} were observed, sufficient information was available to over determine all of the magnetizations (σ, σ_{nn}, $\sigma^x{}_{\mathrm{nnn}}$, $\sigma^y{}_{\mathrm{nnn}}$). The results are shown in Fig. 11.

Within experimental error we found $\sigma^x{}_{\mathrm{nnn}}(T)\equiv\sigma^y{}_{\mathrm{nnn}}=\sigma_{\mathrm{nnn}}$ and thus in the figure only σ_{nnn} is plotted. (In fact, all of our impurity studies are consistent with the identity of $\sigma^x{}_{\mathrm{nnn}}$ and $\sigma^y{}_{\mathrm{nnn}}$.) We believe their equality to be a simple consequence of the additive properties of the superexchange interaction between more than two adjacent ions. In MnF_2:Zn since the nnn magnetization is completely determined from the type II resonance [see Eq. (14b)] we can use this result to predict the temperature dependence of some of the dipolar lines. This provides an additional check of the assumption of strong localization as well as the proper identification of the sites.

For the impurities that do have spin and magnetic

moment, full use has to be made of Eqs. (14a)–(14f). As has been mentioned earlier, when the host-impurity moment difference is small (e.g., Fe^{2+}), not all of the impurity-associated lines are resolvable from the main resonance and there would be insufficient information available to determine all of the σ's. This initially prompted us to make what might at first appear to be an entirely unreasonable assumption, namely, that $J_{nn}^{\text{host-imp}} \simeq 0$. It is clear that this has the great attraction of rendering σ_{nn} identical to Σ and leaving but σ and σ_{nnn} as unknowns. However, simplicity was not the only motivation in this choice. In the pure crystals, MnF_2 and FeF_2, despite the presence of *two* superexchange linkages through intermediate F^- ions for nn magnetic ions as compared with only *one* for nnn, it is found that $|J_{nn}| \ll |J_{nnn}|$.[7,19] (For all practical purposes, in making thermodynamic analyses in MnF_2 and FeF_2 the choice of $J_{nn} \equiv 0$ produces fits to the data that are as satisfactory as obtained from J_{nn} very small and slightly different values of J_{nnn}.) We find for the impure crystal that the choice $J_{nn}^{\text{host-imp}} \simeq 0$ is untenable, resulting in inconsistencies in the analysis of the experimental data. When the assumption $J_{nn}^{\text{host-imp}} \simeq 0$ is abandoned an entirely consistent interpretation of the data may be obtained for Ni, Fe, Co, and V. In fact, as we shall see later on, $J_{nn}^{\text{host-imp}}$ and $J_{nnn}^{\text{host-imp}}$ are comparable in magnitude, although sometimes of opposite sign.

A word or two concerning the analyses of each of the magnetic impurities is in order. As seen in Table IV for the Ni impurity, a large number of resonances are observed in the temperature region of interest, thereby permitting an overdetermination of the various σ's. This provides both a check on the requirement that $J_{nn}^{\text{host-imp}}$ is sizable and that the localization of the magnetic disturbance, originally assumed, is indeed observed. The Fe^{2+} and Co^{2+} cases proved to be difficult to analyze because, for both, only the resonances ν^{I} and ν^{II} were observed. The absence of dipolar lines results from the smallness of $\mu_{Mn}-\mu_{imp}$ in each instance. Fortunately in the MnF_2:Fe there was available Mössbauer-effect measurements of the temperature dependence of the Fe^{57} hyperfine interaction.[20] Combining this direct measurement of $\sigma(T)$ with our observation, we were able to obtain both $\sigma_{nn}(T)$ and $\sigma_{nnn}(T)$ unambiguously. For the Co^{2+} impurity we could not independently determine σ, σ_{nn}, and σ_{nnn}. However, knowing that MnF_2:Co represents a case of a strongly coupled impurity,[5] it is evident from our data that $J_{nn}^{\text{Mn-Co}}$ is significantly different from zero. The V^{2+} impurity situation is somewhat unusual. For MnF_2:V the point-group symmetry of the crystal field is approximately O_h, and the electrons in the $3d^3$ configuration occupy $d\epsilon$ orbitals. But to a $d\epsilon$ orbital only p_π ligand functions may be augmented to construct a molecular orbital.[21] However, it is the $d\gamma$ orbitals which allow s and p_σ ligand augmentation resulting in the large transferred hyperfine interaction—because of the relatively large s contact hyperfine interaction. Since there are no $d\gamma$ orbitals occupied by $3d^3$ in O_h symmetry, the A_i's are much smaller than they are for any of the ions for which the configuration is $3d^n$, with $4 \leq n \leq 9$. In particular, $A_i^{II} \ll A_{Mn}^{I}$ and the error due to using pure MnF_2 A^I values in determining the vanadium magnetization will be sufficiently large to make it impractical [see Eq. (15)]. However, as all dipolar lines are available, one may determine σ_{nn} and σ_{nnn}. The resulting magnetizations for the Ni, Fe, and V impurities are shown in Fig. 12.

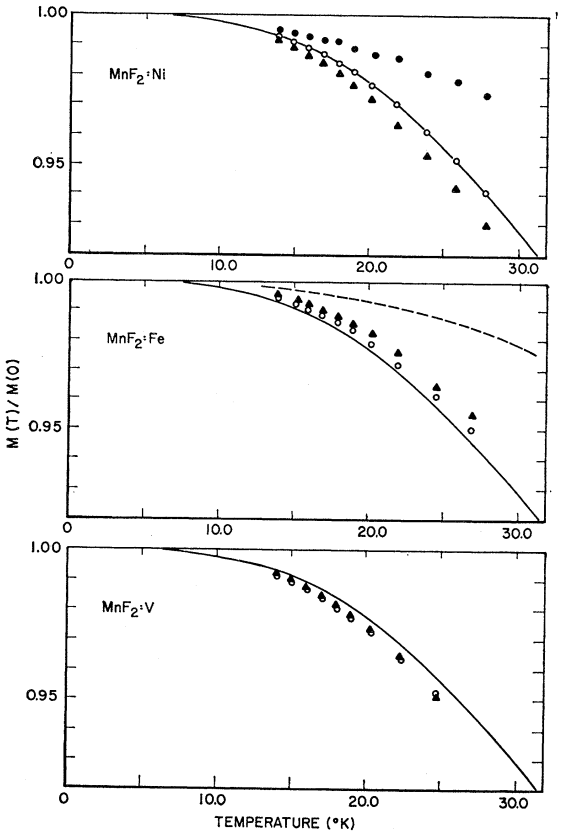

FIG. 12. The normalized magnetizations as deduced from our experiments for the impurity (●), nn (▲), and nnn (○) sites in MnF_2:Ni, MnF_2:Fe, and MnF_2:V. The solid line in each case is the host magnetization. The dashed line in the middle figure is the Fe^{2+} magnetization taken from Ref. 20 and was used in analysing our data.

2. *Parallel Susceptibility—$\chi''(T)$*

Although all of the measurements used to obtain the quantities discussed in the last section actually were made in a magnetic field H, the magnetizations were

[19] H. J. Guggenheim, M. T. Hutchings, and B. D. Rainford, J. Appl. Phys. **39**, 1120 (1968).

[20] G. K. Wertheim, H. J. Guggenheim, and D. N. E. Buchanan, J. Appl. Phys. **40**, 1319 (1969).

[21] A. M. Clogston, J. P. Gordon, V. Jaccarino, M. Peter, and L. R. Walker, Phys. Rev. **117**, 1222 (1960).

corrected to $H=0$, at any given T. Of course, the sublattice magnetization in an antiferromagnet is a function of H as well as T and is strongly anisotropic. Furthermore, in the imperfect crystal there will be a spatial variation in the field dependence of the magnetization associated with the presence of the impurity. It is this property, the local susceptibility, which is particularly amenable to study using the NMR method and which is now our concern.

We consider first the perfect crystal and restrict ourselves to the external field H applied parallel to the c axis. In this case, the magnetization induced by the field, the F^{19} hyperfine field and H itself are all parallel. Therefore, the frequency for resonance is simply obtained from the scalar relation[11]

$$\nu^{19}(T,H)=\sum_{i=\mathrm{I},\mathrm{I}',\mathrm{II}} A_z{}^i S^i \frac{M_i(T,H)}{M_i(0,0)} +\gamma^{19}\left(\sum_j H_D{}^j \frac{M_j(T,H)}{M_0(0,0)}+H\right), \quad (16)$$

where $H_D{}^j$ is the dipolar field at the nucleus in question generated by a Mn^{2+} spin at $r_{j'}$ with j' *not* one of the three nn. The parallel magnetization $M(T,H)$ in an antiferromagnet may be expanded in a Taylor series about $H=0$.

$$M(T,H)=M(T,0)+\left.\frac{\partial M(T,H)}{\partial H}\right|_{H=0} H+\cdots. \quad (17)$$

As $\partial M(T,H)/\partial H|_{H=0}=\chi''(T)$ the parallel susceptibility and for $H\ll(2H_AH_E)^{1/2}$ one need only consider the first term in the expansion,[22] then the frequency for resonance may be written as

$$\nu^{19}(T,H)=\nu^{19}(0,0)\frac{M(T,0)}{M(0,0)} +\left\{\gamma^{19}+\left[(2A_z{}^{\mathrm{I}}+A_z{}^{\mathrm{II}})S^{\mathrm{Mn}}+\gamma^{19}\sum_j H_D{}^j\right]\frac{\chi''(T)}{M(0,0)}\right\}H \quad (18a)$$

or

$$\nu^{19}(T,H)=\nu^{19}(T,O)+\gamma^{19}H[1+f(T)], \quad (18b)$$

where $f(T)=[(1/\gamma^{19})(2A_z{}^{\mathrm{I}}+A_z{}^{\mathrm{II}})S+\sum_j H_D{}^j]\chi''(T)/Ng\beta S$ is the *fractional* shift in the field dependence of the F^{19} NMR frequency. From this it is evident that a measurement of frequency versus field gives $\chi''(T)$ directly. We have made such a measurement in pure MnF_2 at 20.3°K and find $\chi''(T)=(1.33\pm0.05)\times10^{-4}$ compared with a value of 1.33×10^{-4} obtained from bulk susceptibility measurements made in the normal manner.[23] The absolute accuracy of this technique is, of course, limited by how precisely the resonant frequency may be determined and the accuracy of the hyperfine coupling constants. However, the sensitivity of the technique is only limited by the precision of the resonant-frequency determination which for MnF_2 gives us a sensitivity $\Delta\chi''=10^{-6}$.

The real value of this technique is apparent in measuring *local* susceptibilities in the impure crystal. For impurities in MnF_2 with an applied field parallel to the c axis, expression (16) may be generalized to

$$\nu^{19}(T,H)=A_z{}^{\mathrm{I}}S^{\mathrm{I}}\frac{M_{\mathrm{I}}(T,H)}{M_{\mathrm{I}}(0,0)} +A_z{}^{\mathrm{I}'}S^{\mathrm{I}'}\frac{M_{\mathrm{I}'}(T,H)}{M_{\mathrm{I}'}(0,0)}-A_z{}^{\mathrm{II}}S^{\mathrm{II}}\frac{M_{\mathrm{II}}(T,H)}{M_{\mathrm{II}}(0,0)} +\gamma^{19}\sum_j H_D{}^j\frac{M_j(T,H)}{M_j(0,0)}+\gamma^{19}H, \quad (19)$$

where the next to the last term is just the dipolar contribution from the rest of the crystal. Again taking the change in the magnetization to be linear in H and keeping in mind the relative signs of the applied field and spin directions, we find

$$\nu^{19}(T,H)=A_z{}^{\mathrm{I}}S^{\mathrm{I}}\frac{M_{\mathrm{I}}(T,0)}{M_{\mathrm{I}}(0,0)}+A_z{}^{\mathrm{I}'}S^{\mathrm{I}'}\frac{M_{\mathrm{I}'}(T,0)}{M_{\mathrm{I}'}(0,0)} -A_z{}^{\mathrm{II}}S^{\mathrm{II}}\frac{M_{\mathrm{II}}(T,0)}{M_{\mathrm{II}}(0,0)}+\gamma^{19}\sum_j H_D{}^j\frac{M_j(T,0)}{M_j(0,0)} +\left[\gamma^{19}+A_z{}^{\mathrm{I}}S^{\mathrm{I}}\frac{\chi_{\mathrm{I}}''(T)}{M_{\mathrm{I}}(0,0)}+A_z{}^{\mathrm{I}'}S^{\mathrm{I}'}\frac{\chi_{\mathrm{I}'}''(T)}{M_{\mathrm{I}'}(0,0)} +A_z{}^{\mathrm{II}}S^{\mathrm{II}}\frac{\chi_{\mathrm{II}}''(T)}{M_{\mathrm{II}}(0,0)}+\gamma^{19}\sum_j H_D{}^j\frac{\chi_j''(T)}{M_j(0,0)}\right]H. \quad (20)$$

Therefore, just as we have shown with the various temperature dependencies of the zero-field magnetizations of the impurity and neighboring sites, one may determine the *local* susceptibilities of the impurity and neighboring sites by studying the field dependencies of the impurity-associated resonances. Because of the strong impurity-induced line broadening mentioned in the previous section the sensitivity is reduced when compared to pure MnF_2. For this reason it is very difficult to measure the relatively small susceptibilities of the strongly coupled impurities. But a weakly coupled impurity or the neighbors to a spinless impurity are more favorable candidates. The case of MnF_2:Zn is an example of the latter. Zn^{2+} being a nonmagnetic impurity, the frequency for resonance of the type II F^{19}

[22] J. A. Eisele and F. Keffer, Phys. Rev. 96, 929 (1954).
[23] Charles Trapp and J. W. Stout, Phys. Rev. Letters 10, 157 (1963).

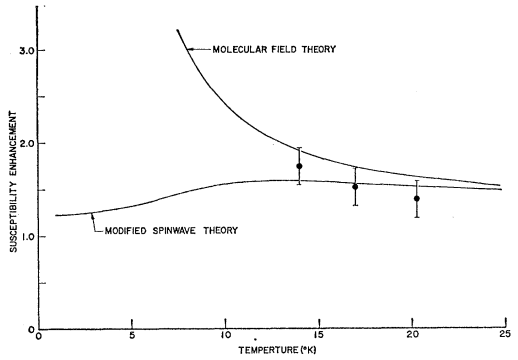

FIG. 13. The enhancement of the local susceptibility at the nnn site to the spinless impurity in MnF_2:Zn. The solid lines are theoretical models discussed in the text.

nuclei is given by

$$\nu_{II}^{19}(T,H)=2A_z{}^{I}S^{Mn}\sigma_{nnn}(T)+\gamma^{19}\sum_j H_D{}^j\Sigma(T)+\left[\gamma^{19}+\frac{2A_z{}^{I}S^{Mn}\chi_{nnn}{}''(T)}{M_{nnn}(0,0)}+\gamma^{19}\sum_j H_D{}^j\frac{\chi_j{}''(T)}{M_j(0,0)}\right]H, \quad (21)$$

where

$$\sigma_{nnn}(T)=M_I(T,0)/M_I(0,0)$$

and

$$\Sigma(T)=M_{host}(T,0)/M_{host}(0,0)\,.$$

Hence, with a measurement of $\nu_{II}^{19}(T,H)$, we directly obtain the local susceptibility in that part of the crystal which is most strongly affected by the impurity. The results of this measurement are shown in Fig. 13. The susceptibility enhancement of the nnn site χ_{nnn}/χ_{pure} is plotted as a function of temperature, from which it is clear the Zn has a strong effect on $\chi''(T)$ at the nnn site. There are also shown various calculated enhancements which will be discussed later.

3. *Nuclear Spin-Lattice Relaxation*

Another measureable quantity which is sensitive to the thermodynamics of the system is T_1, the longitudinal relaxation time. T_1 in pure $MnF^{19}{}_2$ arises from the Raman scattering of magnons.[24] We have studied T_1 for a number of the impurity-associated resonances as a function of temperature. Since the difference between the T_1's of the impurity-associated resonances and T_1 in pure $MnF^{19}{}_2$ is small compared to the temperature variation of either one (they vary by six orders of magnitude over the range 4–30°K), we have examined the ratio $T_1{}^{pure}/T_1{}^{impure}$. These results are presented in Table V. In addition to these results the T_1 of the main resonance in the impurity-doped samples was measured and found to agree with the T_1 of pure MnF_2, within experimental error. This implies the effect on T_1 of the impurity-associated resonances may be ascribed to local distortions of the spin-wave spectrum in the immediate vicinity of the impurity rather than changes in the bulk properties of the crystal. We pursue this point in the next section.

[24] N. Kaplan, R. Loudon, V. Jaccarino, H. J. Guggenheim, D. Beeman, and P. Pincus, Phys. Rev. Letters 17, 357 (1966).

TABLE V. Longitudinal relaxation of certain of the impurity-associated F^{19} resonances. Because of the rapid variation of T_1 with temperature, which tends to obscure the impurity effects, we give only the ratio of the impurity-associated relaxation *rate* to the pure MnF_2 relaxation rate at 4.2, 14.0, and 20.3°K.

Resonance	4.2(°K)	14.0(°K)	20.3(°K)
Co-I	3.2 ±0.6	2.1 ±0.4	1.0±0.2
Co-II	1.4 ±0.3	1.4 ±0.3	1.0±0.2
Ni-II	0.60±0.12	0.77±0.15	1.0±0.2
Zn-II	2.0 ±0.4	1.2 ±0.2	1.4±0.3
Zn-f	1.2 ±0.2	1.3 ±0.3	1.4±0.3

B. Interpretation

1. *Theory of Impurity-Related $M(T)$*

The temperature dependence of the sublattice magnetization of antiferromagnetic MnF_2, for $T<T_N/3$, has been shown[6] to be accurately predicted by linear spin-wave theory which properly includes zone-boundary effects. The slow decrease of $M(T)$ at temperatures below 10°K reflects the pronounced effects of the gap $E(k=0)$ in the magnon spectrum at the center of the zone. Since $E(k=0)=(2JKS)^{1/2}=k_B(13°K)$, it is evident that $M(T)$ is a sensitive function of the exchange J, the spin S, and the anisotropy K.

Similarly, in the impure crystal, we would expect the temperature dependence of the magnetizations at the impurity and its neighboring sites to provide information concerning the host-impurity ion interactions. In the Heisenberg approximation the Hamiltonian for the spin system is expressed as

$$\mathcal{H}=-\sum J_{il}\mathbf{S}_i\cdot\mathbf{S}_l-\sum K_i(S_i{}^z)^2-\mu_0H_0\sum g_iS_i{}^z, \quad (22)$$

where J_{il} is the pairwise isotropic exchange interaction (between either nn or nnn ions in our system), K_i the single-ion anisotropy constant of the ith ion, and the last term the ith Zeeman energy. In general, the impurity parameters S', J', and K' will differ from the host parameters S, J, and K.

Certain features of the impurity problem may be understood in terms of a qualitative picture of changes that occur in the effective field that acts upon the impurity and its neighboring magnetic sites. For example, in the case of the nonmagnetic impurity (e.g., Zn^{2+}) in MnF_2, each nnn Mn "sees" an effective exchange field that is $\frac{7}{8}$ as large as in pure MnF_2. Therefore, one would expect σ_{nnn} to fall faster than the host magnetization. Similarly, one would expect σ_{nn} to be almost identical to Σ the host magnetization as the effective field at the nn site is only reduced by a small amount because $|J_1|\ll|J_2|$. This is what is observed. These nonmagnetic impurity results point out the useful fact that while the impurity magnetization σ depends

on both J_1^{I-H} and J_2^{I-H}, σ_{nnn} only depends on J_2^{I-H} and σ_{nn} on J_1^{I-H}. Therefore, any differences between σ_{nnn} or σ_{nn} and the host magnetization may be directly attributed to J_2^{I-H} and J_1^{I-H}, respectively. In particular, if the sign and magnitude of the host-impurity exchange is such as to *increase* the effective exchange field, then the corresponding magnetization will be *above* the host magnetization and conversely. Thus, the behaviors of $\sigma_{nn}(T)$ and $\sigma_{nnn}(T)$ relative to those of $\sigma(T)$ and $\Sigma(T)$ enable one to determine the sign and magnitude of J_1^{I-H} and J_2^{I-H}, respectively.

From these considerations we can now qualitatively interpret the results shown in Fig. 12. It is evident from the Ni magnetization that this is a strongly coupled impurity. However, one notes, that in the framework of an effective field picture, since $\sigma_{nnn}=\Sigma$, it is required that $J^{Mn-Mn}S_{Mn}=J^{Mn-Ni}S_{Ni}$. The behavior of $\sigma_{nn}(T)$ can only be explained by an antiferromagnetic J_1^{Ni-Mn} comparable in size to J_2^{Ni-Mn}. Similarly, for MnF_2:Fe, where the impurity is known to be strongly coupled,[20] we find from the behavior of $\sigma_{nnn}(T)$ that $J_2^{Fe-Mn}S_{Fe} > J_2^{Mn-Mn}S_{Mn}$ and from $\sigma_{nn}(T)$ that J_1^{Fe-Mn} is large and ferromagnetic. Unfortunately for MnF_2:V $\sigma(T)$ cannot be directly determined. However, using $\sigma_{nn}(T)$ and $\sigma_{nnn}(T)$ we can tell that $J_2^{V-Mn}S_V < J_2^{Mn-Mn}S_{Mn}$ and that J_1^{V-Mn} is large and antiferromagnetic. Hence, MnF_2:V is a case of a weakly coupled impurity.

The most striking and unexpected feature of these qualitative results is the existence of a significant J_1^{I-H} when nearly all J_1's in the pure iron group fluorides are so small. Subsequent to our preliminary experiments there appeared some indirect evidence that supports these conclusions. Measurements of the concentration dependence of T_N in $Mn_{1-x}Fe_xF_2$ crystals, using Fe^{57} Mössbauer effect, show deviations from a linear dependence significantly larger than in other systems where only one exchange path is possible.[25] The observed dependence is easily explained by the existence of a ferromagnetic J_1^{Fe-Mn} of the magnitude deduced from our experiments. Furthermore, optical studies in Ni:MnF_2[4] interpreted assuming only a J_2-type exchange, show the Mn-Ni exchange to Mn-Mn exchange ratio is smaller that it is in Ni:$KMnF_3$ and Ni:$RbMnF_3$. Again these results are more naturally explained by assuming the existence of an antiferromagnetic J_1^{Ni-Mn} in Ni:MnF_2 of the magnitude deduced from our experiments.

A somewhat more quantitative approach may be made using molecular-field (MF) theory where the exchange interactions are replaced by effective fields. The effective exchange field at site i is then given by

$$\mathbf{H}_i=\mathbf{H}+\sum_j \gamma_{ij}\mathbf{M}_j, \tag{23}$$

where $\mathbf{H}$ is an external field, γ_{ij} is the molecular-field coupling constant, and $\mathbf{M}_j$ the magnetization of site j. Since $\mathbf{M}_j$ depends on $\mathbf{H}_j$, we have a set of coupled equations in the magnetizations. For a pure crystal these equations are easily decoupled as all sites "see" the same effective exchange field. However, such is not the case for impure samples where the effective exchange fields, and thus the magnetizations, vary from site to site. Here the magnetization at site i is given by the well-known expression

$$M_i=g_i\beta S_i B_{S_i}(g_i\beta S_i H_i/kT), \tag{24}$$

with $B_{S_i}(x)$ being the Brillouin function for the spin at site i. Because of the nature of the MF approximation, the elementary excitations of the system are localized to individual sites and have energies solely determined by the effective exchange field at each site. This results in a series of δ functions for the density of states. As discussed previously,[26,27] because of this δ-function density of states, MF theory is quite good at describing weakly coupled impurities, as the local impurity modes are sharp and being low down in the band dominate the thermodynamic properties. Figure 14 shows a strongly coupled impurity as viewed in MF and spin-wave pictures. Here again the impurity mode is adequately described by a MF theory. However, being above the host spin-wave band it does *not* dominate the thermodynamics at low temperatures.[20] It is the inability of MF theory to describe the lower-energy collective excitations which severely limits its applicability.

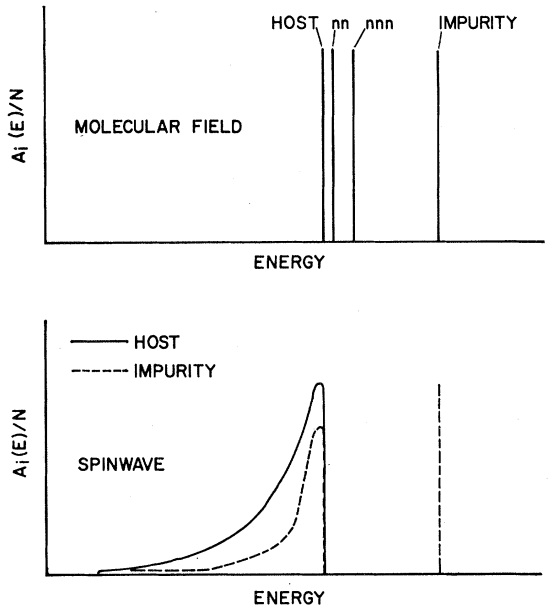

FIG. 14. A schematic representation of the effective density of states for a strongly coupled impurity in the molecular field and spin-wave approximations. The spectral weight function $A_i(E)$ is given for various sites.

[25] G. K. Wertheim, H. J. Guggenheim, M. Butler, and V. Jaccarino, Phys. Rev. **178**, 804 (1969).

[26] V. Jaccarino, L. R. Walker, and G. K. Wertheim, Phys. Rev. Letters **13**, 752 (1964).

[27] H. Callen, D. Hone, and A. Heeger, Phys. Letters **17**, 233 (1965).

TABLE VI. Host-impurity exchange parameters determined from a modified molecular-field model that is discussed in the text.

Impurity	Electronic configuration	Nominal spin	$J_1^{\text{Mn-imp}}$ (°K)	$J_2^{\text{Mn-imp}}$ (°K)
V^{2+}	$3d^3$	$\frac{3}{2}$	−1.0	−1.5
Mn^{2+}	$3d^5$	$\frac{5}{2}$	+0.32[a]	−1.76[a]
Fe^{2+}	$3d^6$	2	+3.1	−3.3
Co^{2+}	$3d^7$	$\frac{3}{2}$	...	...
Ni^{2+}	$3d^8$	1	−2.5	−4.3
Zn^{2+}	$3d^{10}$	0	...	..

[a] From Ref. 7.

As will be seen later, a small change in the effective exchange field results in a shift in the peak of the spin-wave density of states and a small change in the amplitude of the low-energy spin waves. A molecular-field picture adequately describes the shift of the peak, while neglecting the effects on the low-energy spin waves. For this reason a molecular-field pictures of small variations in exchange fields should be successful in regions where the magnetization is dominated by the peak in the spin-wave density of states. Therefore, we would expect a MF theory to be more useful in predicting the change in magnetization at neighboring sites to a strongly coupled impurity than it would be at the impurity site itself, because the *change* in the effective field at the neighboring site is *small* compared to its value in the pure crystal. This is not so for the impurity site.

More explicitly, the changes in magnetization at nn and nnn sites with respect to the host magnetization

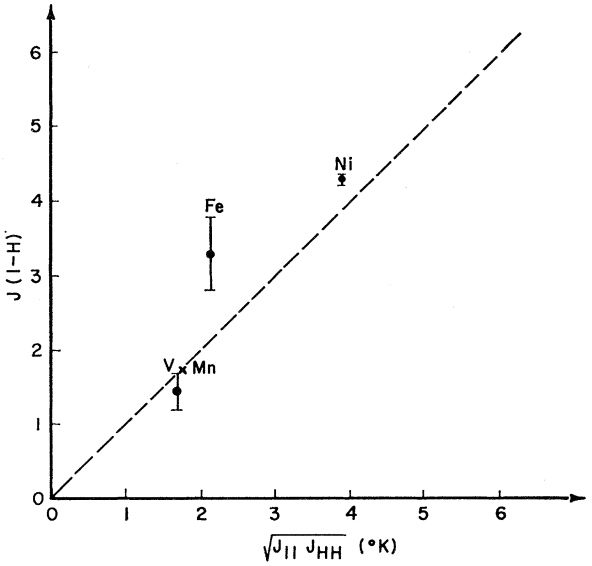

FIG. 15. A plot of the impurity-host intersublattice exchange as determined by our modified molecular-field model versus the geometric mean of the intersublattice impurity-impurity and host-host nnn exchanges. The dashed line is a theoretical result of Ref. 28 for an Anderson superexchange mechanism. This relation is not even approximately obeyed for the intrasublattice nn exchange interactions.

in MnF_2:X have been fit to the following expression:

$$\sigma_{\text{host}}-\sigma_{\text{nn,nnn}}=B_s(x_{\text{host}})-B_s(x_{\text{nn,nnn}})\,. \qquad (25)$$

By adjusting the values of $x_{\text{nn,nnn}}$ to obtain a best fit, the various exchange parameters in Table VI are found. While there are systematic discrepancies between a best fit and experiment (indicating the limitations of molecular-field theory), the exchange parameters obtained are in qualitative agreement with those obtained from other experiments and the more sophisticated theory to be discussed, remembering that ours is a two-parameter (J_1,J_2) theory and all others have been one (J_2). As an additional check on this model, we have fit the nnn magnetization in Zn-doped MnF_2 assuming a Zn spin of 2.5 and $\sigma(T)=1$. The resultant fit, while still exhibiting systematic deviations, yields the expected $J_2^{\text{Mn-Zn}}$ of 0, to three decimal places. It appears from the above comparisons that the model is more useful than one might have expected at first sight. We feel the exchange parameters quoted in Table VI are accurate to plus or minus 30%. The question arises as to whether the values of J_1' and J_2' are reasonable or not from a first-principles point of view. It has been shown[28] that for certain superexchange mechanisms the Anderson theory[29] would predict the unlike ion exchange to be the geometric mean of the like ion exchange interactions. A comparison of $J_2^{\text{imp-host}}$ versus $(J_{\text{II}}J_{\text{HH}})^{1/2}$ for the values of the exchange parameters given in Table VI is plotted in Fig. 15. Interestingly the near-neighbor exchange $J_1^{\text{imp-host}}$ does not even approximately obey this relationship.

While we have found MF theory to be surprisingly useful for treating the impurity problem, it has obvious drawbacks which are only removed by a more sophisticated treatment of the problem. One such approach is the thermodynamic Green's-function technique. This method has been used to treat the thermodynamic properties of pure ferro-[30] and antiferromagnets[31] as well as the impure systems.[32] A detailed theory, applicable to impurities in bcc antiferromagnets in which $J_{\text{nnn}}\gg J_{\text{nn}}$, has been constructed by Hone and Walker (HW).[33] Anisotropy is treated in the random-phase approximation by replacing $\Sigma K(S_i^z)^2$ with $\Sigma K S_i^z\langle S_i^z\rangle$ in Eq. (22). One serious limitation of the HW theory as applied to impurities in MnF_2 is the assumption that $J_{\text{nn}}=0$.

It is difficult to characterize briefly the details of their

[28] G. E. Bacon, R. Street, and R. H. Tredgold, Proc. Roy. Soc. (London) **217**, 252 (1953).
[29] P. W. Anderson, Phys. Rev. **79**, 350 (1950).
[30] D. N. Zabarev, Usp. Fiz. Nauk **71**, 71 (1960) [English transl.: Soviet Phys.—Usp. **3**, 320 (1960)]; S. V. Tyablikov, Ukr. Matem. Zh. **11**, 287 (1959).
[31] M. E. Lines, Phys. Rev. **135**, A1336 (1964); **139**, A1304 (1965).
[32] D. Hone, H. Callen, and L. R. Walker, Phys. Rev. **144**, 283 (1966); D. Hone, in *Localized Magnons and Interactions of Spins with Localized Excitations*, edited by R. F. Wallis (Plenum Press, Inc., New York, 1968).
[33] D. Hone and L. R. Walker (private communication).

theory and it is not our intent to do so. However, one of the quantities that is central to the spectral representation of the Green's function is the so-called spectral weight function $A(\beta,E)$. It may be interpreted in a relatively simple manner. For the perfect crystal $A(\beta,E')$ and the magnon density per spin $n(E')$ are related by

$$(1-e^{-\beta E'})A(\beta,E')=2\langle S^z\rangle n(E'), \tag{26}$$

where the magnon energies E' are normalized to the top of the spin-wave band. In the impure crystal we define a position-dependent reduced spectral weight function $a_i(E')$ at site i (which may or may not be the impurity site)

$$a_i(E')\equiv A_i(\beta,E')\langle S^z\rangle/A(\beta,E')\langle S_i{}^z\rangle, \tag{27}$$

where $(e^{-\beta E}-1)A_i(\beta E)$ is twice the imaginary part of the retarded Green's function. With respect to Eqs. (26) and (27) we may interpret $a_i(E')$ as follows: It is the ratio of the probabilities of finding a spin deviation of energy E' at site i in the impure and pure crystals. While the presence of a single impurity does not significantly affect $n(E')$,[32] it dramatically alters the amplitude of the spin deviation wave function at, and in the immediate vicinity of, the impurity.

The HW calculation of $a_i(E')$ for the nnn to a spinless impurity is given in Fig. 16 and is useful in making comparison with our MnF_2:Zn studies. That $a_{\rm nnn}(E')$ is peaked at $E\simeq\frac{7}{8}E_{\max}$ is simply related to the fact that the $Z=8$ nnn exchange linkages in the perfect crystal are diminished by one for the nnn to the impurity in the imperfect crystal.

Knowledge of $a_i(\beta,E)$ is sufficient to calculate many of the thermodynamic quantities of interest. For example, the magnetization $\langle S_i{}^z\rangle$ is given as

$$\langle S_i{}^z\rangle=S_i-\int[e^{\beta E}-1]^{-1}n(E)a_i(E)dE. \tag{28}$$

For the spinless impurity case in the bcc lattice, HW obtained the results shown in Fig. 11 for the temperature dependence of the magnetization at nnn host sites. These are to be compared with the experimental results in the same figure. Not only is the agreement seen to be excellent here but both theory and experiment show strong localization of the impurity modes since negligible disturbance of the magnetization appears at more distant neighbors. To our knowledge this is the first comparison between experiment and a precise theory for the "impurity" magnetization in an antiferromagnet where all of the parameters are accurately known.

The reduced spectral weight function $a_i(\beta,E')$ for $S'\neq 0$ has been calculated by HW for a full range of values of J'/J from which $\langle S_i{}^z\rangle$ has been obtained. Since our experiments clearly indicate $|J_{\rm nn}|$ to be comparable to $|J_{\rm nnn}|$ and their theory presumes $J_{\rm nn}\equiv 0$, any comparison, that may be made, must be qualitative

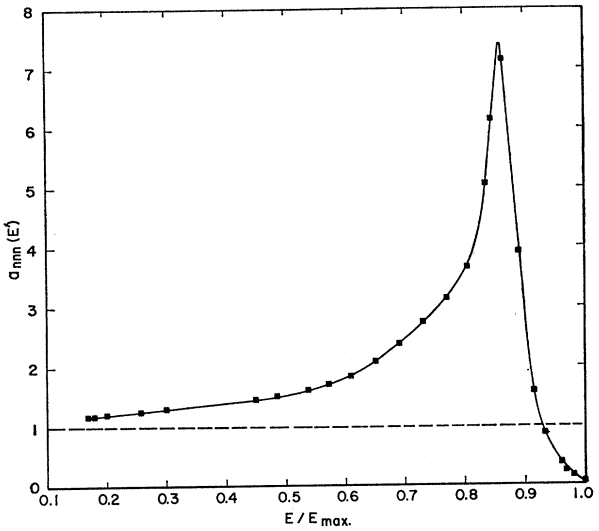

FIG. 16. The reduced spectral weight function for the nnn site to the impurity in MnF_2:Zn as calculated by Hone and Walker (Ref. 33). The energy is normalized to the top of the spin-wave band.

in nature.[34] Bearing this in mind we compare our results for $Ni^{2+}(S'=1)$ in MnF_2 with their calculations for the impurity and nnn magnetizations in Fig. 17. Certain features of this figure are worth commenting upon. The theoretical curves both for the nnn as well as the nn magnetizations approximately coincide with that of the pure host. This is entirely accidental and results from

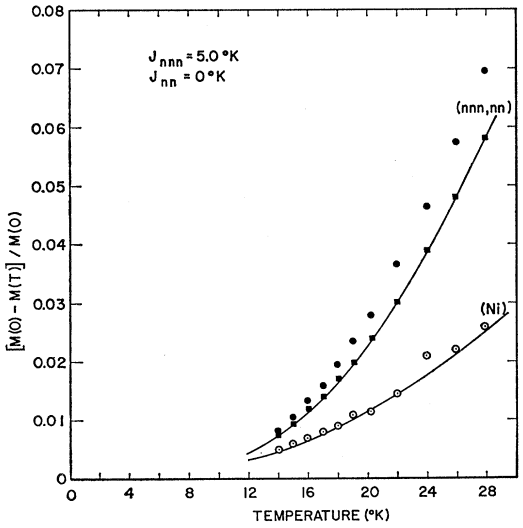

FIG. 17. The observed deviations of the reduced magnetization from unity for Ni(○), nnn(■), and the nn(●) sites in MnF_2:Ni are compared to the deviations calculated by Hone and Walker using the host-impurity exchange parameters shown. Their calculated curves for the nn and nnn sites accidentally coincide in the temperature range of interest.

[34] A theoretical study of the effects of $J_{\rm nn}$ on the local modes has recently been completed by E. Shiles and D. Hone. However, application of these results to calculate thermodynamic properties of the impurity system have not yet been performed.

the particular value of J'/J and S' used in the interpretation. Our experimental results for the nn magnetization clearly do not agree with their restrictive theory. This shows the importance of knowing as much as possible about the spatial distribution of the magnetization and how one might easily be misled by measuring only the impurity magnetization.

2. Theory of Local Susceptibility

As remarked earlier, the *local* susceptibility at an impurity and neighboring sites may be determined from measurements of the various impurity-associated F^{19} NMR frequencies versus applied field H. More precisely, what is obtained directly from our experiments is the enhancement of the local susceptibility relative to that of the unperturbed host. In view of this, we recall certain features of the pure-MnF_2 $\chi''(T)$ which have been studied by more conventional techniques.[23] Because of the gap (kT_{AE}) in the magnon spectrum at $\mathbf{k}=0$, $\chi''(T)$, which is 0 at 0°K, remains extremely small for $T\ll T_{AE}=13.5$°K. It rises rapidly thereafter until at $T_N=67.3$°K it achieves a value of $\chi''(67.3)=1.1\times10^{-3}$.[35] Of course, the monotonic increase of $\chi''(T)$ with T is associated with the increasing number of thermal magnons that are generated at higher T.

Perhaps the simplest local susceptibility to understand is that of the neighbors to a spinless impurity (e.g., Zn^{2+} in MnF_2). As was argued previously for $\langle S^z\rangle_{\text{nnn}}$, we would expect $\chi''_{\text{nnn}}(T)$ at the nnn site to a Zn impurity to be larger than the host susceptibility because the reduced number of exchange linkages makes it easier to create spin deviations at these more weakly coupled spins. A semiquantitative description of χ''_{loc} may be obtained from a molecular-field model. In this model the magnetization at site i is given by

$$M_i=g\beta S_i B_{S_i}(y_i), \tag{29}$$

where the argument of the Brillouin function is $y_i=(g\beta S_i/kT)H_i$ and H_i is the effective field acting at site i. The parallel susceptibility χ_i'' may be obtained by expanding $B(y_i)$ about $H=0$ keeping only terms linear in H[36]:

$$\chi_i''H=g_i\beta S_i\left[\frac{dB(y_i)}{dy_i}\right]_{H=0}\frac{y_i}{H_i}\frac{\partial H_i}{\partial H}H. \tag{30}$$

As

$$H_i=H+\frac{2}{g_i\beta}\sum_j J_{ij}S_j\frac{M_j}{M_j^0},$$

we may express χ_i'' as

$$\chi_i''=kT\left(\frac{y_i}{H_i}\right)^2\left[\frac{dB(y_i)}{dy_i}\right]_{H=0}\times\left[1+\frac{2}{g_i\beta M_j^0}\sum_j J_{ij}S_j\chi_j''\right], \tag{31}$$

which is a system of coupled equations. The equations may be decoupled by setting $\chi_j''=\chi_i''$. The error this introduces will be small providing $2\sum J_{ij}S_j\chi_j''/g_i\beta M_j^0\ll1$. This inequality is easily seen to be satisfied by reexpressing it in the form $(E_{\text{ex}}/E_{H_0})(\chi_j''H_0/M_j^0)\ll1$. For MnF_2 the ratio of the exchange to external field energies is ~100 at ~7 kG, $M_j^0\sim1.2$ kG, and $\chi_j''H_0\sim7\times10^{-4}$ kG. Thus, at the highest temperature of interest (30°K) the maximum error is $\leq2\%$, if χ_j'' is replaced by χ_i'' in Eq. (31). Within this decoupling approximation

$$\chi_i''(T)=\frac{g_i^2\beta^2S_i^2\left[dB(y_i)/dy_i\right]_{H=0}}{kT-\sum_j J_{ij}S_jS_i\left[dB(y_i)/dy_i\right]_{H=0}}. \tag{32}$$

A comparison of Eq. (32) with experiment is made in Fig. 13. Note that the susceptibility enhancement predicted by molecular-field theory diverges as T approaches zero, even though the susceptibility vanishes asymptotically. This results from the δ-function-like density of states inherent to the molecular-field theory. In the low-temperature limit the enhancement factor behaves as $\exp(\Delta/kT)$, where Δ is the difference between the exchange energies for an ion in pure MnF_2 and at the impurity site. One interesting feature is that molecular-field theory appears to work so well above 20°K. We believe this to be a consequence of the fact that the thermodynamics is dominated by the peak in the density of states and this is adequately described in the molecular-field approximation.

We would expect a more exact description of the enhancement to be obtainable from HW's thermodynamic Green's-function approach. In linear spin-wave theory

$$\langle S_z{}^i\rangle=S_i-\langle n_i\rangle \tag{33}$$

(apart from the coherence factors that also enter into the zero-point deviation in the antiferromagnet), where n_i is the spin deviation number operator. In a pure material the probability of finding such an excitation at any site is proportional to $1/N$. However, the impurity destroys the translational symmetry of the crystal and makes the probability of finding such excitations near the impurity different from what it is in the rest of the crystal. The enhancement of the probability of finding a spin deviation of energy E at site i is just $a_i(E)$, the reduced spectral weight function. Hence, to calculate a particular thermodynamic quantity for the impurity-associated problem, we require that wherever the density of states appears it should be multiplied by the $a_i(E)$ appropriate to the site in question. Applying this rule to the parallel susceptibility yields the following expression:

$$\chi_i''(T)=\frac{Ng^2\beta^2}{kT}\int_{E_{\min}}^{E_{\max}}\frac{e^{E/kT}}{\left[e^{E/kT}-1\right]^2}n(E)a_i(E)dE, \tag{34}$$

[35] M. Griffel and J. W. Stout, J. Chem. Phys. **18**, 1455 (1950).
[36] J. S. Smart, *Effective Field Theories of Magnetism* (W. B. Saunders Co., Philadelphia, 1966).

where $n(E)$ is the linear spin-wave-theory density of states for pure MnF_2. The results of such a calculation are compared with experiment in Fig. 13. While the experimental errors are large, it is obvious that an enhancement of the local susceptibility of approximately the right amount is observed. The interesting dropoff below about 12°K predicted by the spin-wave theory, which unfortunately is difficult to measure experimentally because of the rapid decrease in the absolute parallel susceptibility, is caused by the gap (kT_{AE}) in the MnF_2 spin-wave spectrum. As the temperature decreases below (T_{AE}), lower and lower energy magnons dominate the contribution to the susceptibility, until in the limit of zero temperature the enhancement goes to $a_i(E_{\text{gap}})$, the value of the reduced spectral weight function at the gap energy and, of course, $\chi'' \to 0$. As the temperature is increased above (T_{AE}), the zone-boundary magnons rapidly become more important because of their larger density of states. However, the impurity $a_i(E)$ is much less than unity at the zone boundary and relative to the pure crystal tends to reduce the zone-boundary contribution. There results a slow decrease in the enhancement at higher temperatures.

3. *Interpretation of* T_1

Additional information about the localized impurity modes may be obtained from nuclear spin-lattice relaxation (NSLR) measurements. As a background to the impurity-associated T_1 problem, we briefly review the origin of T_1 in pure MnF_2. Direct processes, in which a magnon is absorbed or emitted and a nuclear spin is flipped, are energetically forbidden because the nuclear Zeeman energy is so much smaller than the minimum magnon energy $E(\mathbf{k}=0)$. It was shown[24] that zero-field NSLR in pure MnF_2 proceeds via a two-magnon Raman-scattering process. That is to say, a magnon at energy E and momentum $\mathbf{k}$ interacts with a nucleus through the hyperfine coupling. The nucleus changes its z component of spin by one unit and a magnon of energy E' and momentum $\mathbf{k}'$ is emitted. This requires that the x or y component of nuclear spin (I_x or I_y) couple to some component of electronic spin. As only S_z, when expressed in spin-wave-operator form, has terms which simultaneously create and destroy magnons and would therefore correspond to two-magnon processes, the important terms in the hyperfine coupling tensor must be A_{yz} and A_{xz}. These off-diagonal terms arise mainly from the dipolar fields of the spins at sites I and I'[21] (see Fig. 2). Although the symmetry of the crystal requires that the static fields at the fluorine sites arising from the off-diagonal terms cancel, the dynamic field effects that are involved in relaxation do not vanish. The resultant two-magnon relaxation rate is expressible as[24]

$$\left(\frac{1}{T_1{}^0}\right)=\left(\frac{\pi}{\hbar^2 N}\right)(A_{yz}{}^{\mathrm{I}})^2\sum_{\mathbf{k}\mathbf{k}'}(u_{\mathbf{k}}{}^2u_{\mathbf{k}'}{}^2+v_{\mathbf{k}}{}^2v_{\mathbf{k}'}{}^2)\times\left\{\frac{e^{E_{\mathbf{k}}/kT}}{[e^{E_{\mathbf{k}}/kT}-1]^2}\right\}\{2-2\cos[(\mathbf{k}-\mathbf{k}')\cdot(\mathbf{r}^{\mathrm{I}}-\mathbf{r}^{\mathrm{I}'})]\}\times\delta(E_{\mathbf{k}}-E_{\mathbf{k}'}),\quad(35)$$

where the notation is that used in Ref. 24. This relaxation rate varies over six orders of magnitude from 3 to 30°K, because the temperature region spans the gap in the spin-wave energy spectrum.

Turning now to the impurity-associated problem, we might expect from the above that significant changes in T_1 would occur when the impurity occupies any one of the three adjacent sites to a given F^- ion. From the impurity T_1 data (Table V) three definite effects are observed. The Co-I and Zn-II relaxation rates get more rapid than the host rate at lower temperatures and the Ni-II relaxation rate gets less rapid than the host rate at lower temperatures.

These effects may be explained qualitatively by considering the various F^{19} environments as shown in Fig. 10. As only sites I and I' contribute to the relaxation, the e resonance relaxation should be the same as the host. The relaxation of the f and l resonances will depend, respectively, on how $J_2{}^{\text{host-imp}}$ and $J_1{}^{\text{host-imp}}$ affect the spin waves at the nn and nnn sites. The relaxation of the c resonance is identical with that of the II resonance and both depend on the strength of $J_2{}^{\text{host-imp}}$. If the exchange coupling is weak, as occurs for Zn, the excitation of spin waves at the nnn site is made easier. Since the more excitations there are present the faster is the relaxation, one expects the Zn-II resonance to relax faster than does the host resonance. Indeed this is what is observed at 4.2°K. Similarly, since the Ni spin is strongly coupled to the host, one expects fewer spin waves at the nnn site and correspondingly a slower relaxation in this instance. Again this is just what is observed at 4.2°K. However, in these two cases, the ratios approach unity at higher temperatures for reasons that are not completely obvious.

The type I resonance is a much more complicated problem. Besides drastic modification of the spectral weight function at the impurity and nn sites, it is generally true that $A_{yz}{}^{\mathrm{I}}\neq -A_{yz}{}^{\mathrm{I}'}$ and hence the angular factor $\{2-2\cos[(\mathbf{k}-\mathbf{k}')\cdot(\mathbf{r}^{\mathrm{I}}-\mathbf{r}^{\mathrm{I}'})]\}$ in the zero-field relaxation rate of Eq. (35) does not vanish as $\mathbf{k}\to 0$. Both this complication and the fact that contributions from the $A_{zz}\mathrm{I}_z S_z$ term due to canting of the F^{19} quantization direction may lead to enhancement of the impurity-I relaxation rate at lower temperatures. Two cases need to be distinguished for the type I problem. First, when $|A_{yz}{}^{\mathrm{I}'}S_z{}^{\mathrm{I}'}|$ is either much greater or much smaller than $|A_{yz}{}^{\mathrm{I}}S_z{}^{\mathrm{I}}|$, the hyperfine field is no longer parallel with the z axis so that the angle θ between the electronic and nuclear quantization direction might be

sizable. An example of this occurs with a Ni^{2+} impurity at the type I site. The second case arises when $|A_{yz}{}^{I'}S_z{}^{I'}|\simeq|A_{yz}{}^{I}S_z{}^{I}|$ and hence $\theta\simeq 0$. The nonparallel situation $\theta\neq 0$ not only leads to terms involving $A_{zz}{}^2\sin^2\theta$ (as in the case of the pure crystal when a field is applied perpendicular to the c axis) but to cross terms involving products of diagonal and off-diagonal components of $\bar{A}$. These latter terms accidentally cancel in the pure crystal. They are complicated to treat in even an approximate fashion and since we have not studied an impurity-I relaxation rate appropriate to this case, we will not discuss it further.

The approximately parallel case, as exemplified by Co^{2+}, may be treated in a manner similar to that which was done for the pure crystal. Provided θ is very small, the primary contribution to the two-magnon nuclear relaxation arises from the terms involving only $A_{yz}{}^{I}$ and $A_{yz}{}^{I'}$. The pure-crystal relaxation may be generalized to include the case of $S_z{}^{I'}\neq S_z{}^{I}$ (despite the fact that $|A_{yz}{}^{I'}S_z{}^{I'}|-|A_{yz}{}^{I}S_z{}^{I}|\ll|A_{yz}{}^{I}S_z{}^{I}|$) in the following manner. Defining the ratio

$$|A_{yz}{}^{I'}/A_{yz}{}^{I}|\equiv\eta\,, \tag{36}$$

we may write the relevant perturbation Hamiltonian as

$$\mathcal{H}'=A_{yz}{}^{I}I_y(\delta S_z{}^{I}-\eta\delta S_z{}^{I'})\,. \tag{37}$$

From Fermi's golden rule for the transition probability we find, for the relaxation rate,

$$\frac{1}{T_1}=\frac{\pi}{\hbar}[A_{yz}{}^{I}]^2\sum_f|\langle f|\delta S_z{}^{I}-\eta\delta S_z{}^{I'}|i\rangle|^2\delta(E_f-E_i)\,, \tag{38}$$

where i and f refer to the initial and final states and the specifically nuclear part of the matrix elements have already been evaluated. The corresponding expression in terms of boson operators is

$$\frac{1}{T_1}=\frac{\pi}{\hbar}[A_{yz}{}^{I}]^2\sum_f\times|\langle f|a_I{}^\dagger a_I-\eta a_{I'}{}^\dagger a_{I'}|i\rangle|^2\delta(E_f-E_i)\,. \tag{39}$$

At this point in the perfect lattice because the eigenfunctions are plane waves one normally Fourier transforms to $\mathbf{k}$ space. However, the impure system lacks the translational symmetry of the perfect lattice and the true wave functions are not known. The relaxation rate may be expressed in terms of a complete set of states in $\mathbf{k}$ space:

$$\frac{1}{T_1}=\frac{\pi}{\hbar N^2}[A_{yz}{}^{I}]^2\sum_{\mathbf{k},\mathbf{k}'}|\langle f_s|\varphi_{\mathbf{k}}(\mathbf{r}_I)\varphi_{\mathbf{k}'}{}^*(\mathbf{r}_I)a_{\mathbf{k}}{}^\dagger a_{\mathbf{k}'}-\eta\varphi_{\mathbf{k}}(\mathbf{r}_{I'})\varphi_{\mathbf{k}'}{}^*(\mathbf{r}_{I'})a_{\mathbf{k}}{}^\dagger a_{\mathbf{k}'}|i_s\rangle|^2\delta(E_f-E_i)\,, \tag{40}$$

where $\varphi_{\mathbf{k}}(\mathbf{r})$ are the true magnon wave functions. Making the normal transformation to diagonalize the Hamiltonian,[6] and evaluating the boson-number operators one finally obtains an expression of the form

$$\frac{1}{T_1}=\frac{\pi}{\hbar N^2}[A_{yz}{}^{I}]^2\sum_{\mathbf{k},\mathbf{k}'}(U_{\mathbf{k}}{}^2U_{\mathbf{k}'}{}^2+V_{\mathbf{k}}{}^2V_{\mathbf{k}'}{}^2)\frac{e^{E_{\mathbf{k}}/kT}}{(e^{E_{\mathbf{k}}/kT}-1)^2}\times\{|\varphi_{\mathbf{k}}(\mathbf{r}_I)|^2|\varphi_{\mathbf{k}'}(\mathbf{r}_I)|^2+\eta^2|\varphi_{\mathbf{k}}(\mathbf{r}_{I'})|^2|\varphi_{\mathbf{k}'}(\mathbf{r}_{I'})|^2-\eta[\varphi_{\mathbf{k}}(\mathbf{r}_I)\varphi_{\mathbf{k}}{}^*(\mathbf{r}_{I'})\varphi_{\mathbf{k}'}{}^*(\mathbf{r}_I)\varphi_{\mathbf{k}'}(\mathbf{r}_{I'})+\varphi_{\mathbf{k}}{}^*(\mathbf{r}_I)\varphi_{\mathbf{k}}(\mathbf{r}_{I'})\varphi_{\mathbf{k}'}(\mathbf{r}_{I'})\varphi_{\mathbf{k}'}{}^*(\mathbf{r}_{I'})]\}\delta(E_f-E_i)\,. \tag{41}$$

Note the similarity to the expression for the zero-field relaxation in pure MnF_2. This equation will reduce to the pure MnF_2 expression when $\eta\rightarrow 1$ and $\varphi_{\mathbf{q}}(\mathbf{r}_i)=e^{i\mathbf{q}\cdot\mathbf{r}_i}$. As remarked above, the true wave functions are not known so this problem cannot be solved at present. All that we do know are the spectral weight functions $|\varphi_{\mathbf{k}}(\mathbf{r}_i)|^2=A_i(E)$. Thus what is needed, is information about the relative phases of an appropriate set of states. This points up the interesting fact, that NSLR of impurity-associated resonances can indirectly provide information about the phase of the impurity modes. This is entirely due to the F^{19} nucleus being coupled to more than one magnetic site.

The effects of $\eta\neq 1$ can be investigated by letting $\varphi_{\mathbf{q}}(\mathbf{r}_i)=e^{i\mathbf{q}\cdot\mathbf{r}_i}$. For computational simplicity we use the isotropic magnon dispersion model.[37] For reasons given in Ref. 37, this model does not work well for pure MnF_2 (although it does for FeF_2) but we might expect it to be reasonably good for examining ratios of relaxation rates as similar errors will be introduced into both numerator and denominator. With these restrictions, we obtain the following expression for the ratio of impure to pure relaxation rates:

$$\left(\frac{(1/T_1{}^0)_{\text{impure}}}{(1/T_1{}^0)_{\text{pure}}}\right)=\frac{[(1+\eta^2)A-\eta B]}{(2A-B)}\,, \tag{42}$$

where

$$A=\frac{1}{N^2}\sum_{\mathbf{k},\mathbf{k}'}(U_{\mathbf{k}}{}^2U_{\mathbf{k}'}{}^2+V_{\mathbf{k}}{}^2V_{\mathbf{k}'}{}^2)\frac{\exp(E_{\mathbf{k}}/kT)}{[\exp(E_{\mathbf{k}}/kT)-1]^2}\times\delta(E_{\mathbf{k}}-E_{\mathbf{k}'})$$

and

$$B=\frac{2}{N^2}\sum_{\mathbf{k},\mathbf{k}'}(U_{\mathbf{k}}{}^2U_{\mathbf{k}'}{}^2+V_{\mathbf{k}}{}^2V_{\mathbf{k}'}{}^2)\frac{\exp(E_{\mathbf{k}}/kT)}{[\exp(E_{\mathbf{k}}/kT)-1]^2}\times\cos[(\mathbf{k}-\mathbf{k}')\cdot(\mathbf{r}^{I}-\mathbf{r}^{I'})]\delta(E_{\mathbf{k}}-E_{\mathbf{k}'})\,,$$

and the notation is that used in Ref. 37. Using this expression and the constants appropriate to MnF_2, the ratio of impure to pure relaxation rates for various values of η have been calculated and are shown in Fig. 18. As expected the impurity relaxation rate is enhanced at lower temperatures and we find that the greater the deviation of η from unity, the larger the enhancement.

[37] M. Butler, Tin Ngwe, N. Kaplan, and H. J. Guggenheim, Phys. Rev. **184**, 365 (1969).

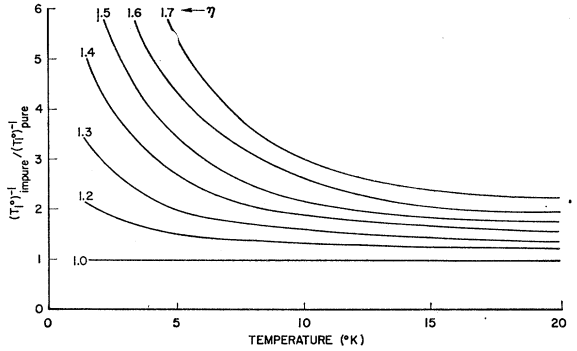

FIG. 18. The enhancement of the two-magnon nuclear spin-lattice relaxation rate due to noncancellation of the A_{yz} terms from the I and I′ sites. η is defined as $|A_{yz}{}^{I'}|/|A_{yz}{}^{I}|$.

Direct comparison of these results with MnF_2:Co is not easily justified. Aside from the approximation of the magnon wave function, the value of η is difficult to determine. While $A_{yz}{}^{I}$ for Co^{++} is not known, it may be estimated by assuming it to be of dipolar origin. It was shown that this is the dominant contribution to $A_{yz}{}^{I}$ in pure MnF_2.[21] If this is done, then η is just the ratio of the spin g values for Mn^{++} and Co^{++} (i.e., the part of the g value which comes from spin and not orbital contributions). This ratio leads to a value of $\eta \sim 1.5$ with which the model predicts enhancement effects of the right magnitude. While these qualitative descriptions are probably correct, a better understanding of the impurity-associated resonance T_1's will require a more precise description of the impurity modes.

V. CONCLUSIONS

We have shown that the local magnon modes, created by the addition of spin impurities to antiferromagnetic MnF_2, are capable of detailed study using NMR techniques. In particular, the localization of the magnetic disturbance in impure MnF_2 and the thermodynamic behavior of the local magnetization, susceptibility and nuclear relaxation are amenable to investigation using the F^{19} NMR and the information previously obtained in the pure crystal.

For the spinless impurity (e.g., Zn^{2+}) the experimental results on the temperature dependence of the magnetization of the impurity nnn spins agrees with the Hone-Walker thermodynamic Green's-function theory. The experimental results for all of the remaining impurities (e.g., Fe, V, Co, Ni) require that one includes an additional nn exchange interaction (between host and impurity) that is of the same magnitude as the dominant nnn exchange. This is in contrast with the host crystal where $|J_{nn}| \ll |J_{nnn}|$. The susceptibility measurements of a nnn to a nonmagnetic impurity have been examined within the framework of a modified spin-wave theory which we believe is capable of explaining differences in χ'' between host and impure crystals. The nuclear relaxation of F^{19} nuclei that are associated directly with the impurity spin gives additional information about the local magnon wave functions and is sensitive to the variation from one site to the next of the phase of these wave functions.

To explain the observed frequency shifts of many of the impurity-associated resonances, we were led to invoke impurity-related strains as the causal mechanism. A semiquantitative theory of the change in the local F^{19} transferred hyperfine field due to such strains is developed in the Appendix. The results of our experiments point to the possibility of a better understanding of local strains in these and other insulating magnetic crystals through application of NMR techniques.

As regards impure crystals of higher concentration, it is clear that the relative intensities of resonances associated with a single impurity and impurity pairs give details of the clustering (or anticlustering) of impurities in these and other crystals. Only briefly examined was the thermodynamic properties of these heavily doped crystals. Since concentrations $>1\%$ produce marked changes in T_N, it would seem worthwhile to study the behavior of the various resonances in the region where $\Delta M/M \to 1$.

Parallel to these investigations of the ordered state (which we are extending to other impure systems, e.g., $X_cRbMn_{1-c}F_3$), it is clear that one should be able to study local susceptibility and dynamic effects associated with the impurity above the transition temperatures. These investigations are currently being pursued at our laboratory.

ACKNOWLEDGMENTS

We are particularly indebted to Dr. D. Hone and Dr. L. R. Walker for numerous discussions concerning their theory of the impurity modes in antiferromagnets and specifically for details of their calculations which we have used in our paper. Their complementary theoretical studies have made possible the large degree of success we have had in interpreting the various thermodynamic properties that we have measured. On a number of occasions we have benefitted from conversations with Dr. P. Pincus and E. Shiles on details of interpretation. We are grateful to the University of California at Santa Barbara Computer Center for providing time on the IBM 360-50 computer.

APPENDIX: IMPURITY-INDUCED STRAIN EFFECTS ON IMPURITY-ASSOCIATED RESONANCES

It was apparent in Sec. III that there are significant differences between the calculated frequency shifts and the observed shifts. We attributed these discrepancies to localized strains at or in the vicinity of the impurity position which cause changes in the transferred hyperfine coupling constants. Here, we first consider the sensitivity of the hyperfine coupling constants to such strains and then treat the strain-induced frequency

shifts for the "dipolar" and "hyperfine" lines in a semiquantitative manner.

For small changes Δr in the Mn^{2+}-F^- separations, one would expect the strain-induced frequency shifts $\Delta\nu$ to be linear in Δr;

$$\Delta\nu_i=\langle S_z^{\mathrm{I}i}\rangle\frac{\partial A_z^{\mathrm{I}i}}{\partial r_{\mathrm{I}}}\Delta r_{\mathrm{I}}+\langle S_z^{\mathrm{I}'i}\rangle\frac{\partial A_z^{\mathrm{I}'i}}{\partial r^{\mathrm{I}'}}\Delta r_{\mathrm{I}'}-\langle S_z^{\mathrm{II}i}\rangle\frac{\partial A_z^{\mathrm{II}i}}{\partial r^{\mathrm{II}}}\Delta r_{\mathrm{II}}, \quad \text{(A1)}$$

where the spins and hyperfine coupling constants are those appropriate to the type I, I′, and II sites with reference to the F^{19} nucleus at site i. The importance of such shifts can be estimated by determining the sensitivity of the A's to the Mn-F distance. One source of this information is the pressure dependence of the F^{19} resonant frequency in MnF_2.[38]

Assume the total hyperfine coupling constant A consists of two parts: (1) the isotropic hyperfine interaction A_{hyp} and (2) the dipolar contribution A_{dip} from the three nearest Mn ions. Then,

$$\frac{\partial A}{\partial P}=\frac{\partial A_{\mathrm{hyp}}}{\partial P}+\frac{\partial A_{\mathrm{dip}}}{\partial P}. \quad \text{(A2)}$$

One may write the hyperfine term more explicitly as the individual contributions from the three neighboring sites.

$$\frac{\partial A}{\partial P}=\frac{\partial A_{\mathrm{hyp}}{}^{\mathrm{I}}}{\partial r^{\mathrm{I}}}\frac{\partial r^{\mathrm{I}}}{\partial P}+\frac{\partial A_{\mathrm{hyp}}{}^{\mathrm{I}'}}{\partial r^{\mathrm{I}'}}\frac{\partial r^{\mathrm{I}'}}{\partial P}-\frac{\partial A_{\mathrm{hyp}}{}^{\mathrm{II}}}{\partial r^{\mathrm{II}}}\frac{\partial r^{\mathrm{II}}}{\partial P}+\frac{\partial A_{\mathrm{dip}}}{\partial P}. \quad \text{(A3)}$$

Since $r_{\mathrm{I}}\approx r_{\mathrm{I}'}\approx r_{\mathrm{II}}$ and the hyperfine interaction is isotropic,

$$\frac{\partial A_{\mathrm{hyp}}{}^{\mathrm{I}}}{\partial r^{\mathrm{I}}}=\frac{\partial A_{\mathrm{hyp}}{}^{\mathrm{I}'}}{\partial r^{\mathrm{I}}}\approx\frac{\partial A_{\mathrm{hyp}}{}^{\mathrm{II}}}{\partial r^{\mathrm{II}}}\equiv\frac{\partial A_{\mathrm{hyp}}{}^{i}}{\partial r^{i}}.$$

This gives us

$$\frac{\partial A_{\mathrm{hyp}}{}^{i}}{\partial r^{i}}=\frac{\partial A/\partial P-\partial A_{\mathrm{dip}}/\partial P}{2\partial r^{\mathrm{I}}/\partial P-\partial r^{\mathrm{II}}/\partial P}. \quad \text{(A4)}$$

Numerical values for all of the necessary quantities may be obtained from Ref. 38. We find the variation of the isotropic hyperfine field with bond length to be

$$\frac{\partial A_{\mathrm{hyp}}{}^{i}}{\partial r^{i}}\approx-56.2\times10^{-4}\ \mathrm{cm^{-1}\ \AA^{-1}}.$$

There only remains to estimate $\partial A_{\mathrm{dip}}/\partial r$ and this can be calculated knowing the radial and angular dependence of the dipolar interaction. We obtain

$$\frac{\partial A_{\mathrm{dip}}{}^{\mathrm{I}}}{\partial r^{\mathrm{I}}}=-3.2\times10^{-4}\ \mathrm{cm^{-1}\ \AA^{-1}},$$

$$\frac{\partial A_{\mathrm{dip}}{}^{\mathrm{II}}}{\partial r^{\mathrm{II}}}=-3.9\times10^{-4}\ \mathrm{cm^{-1}\ \AA^{-1}}.$$

Finally we combine the dipolar and isotropic hyperfine contributions (being careful about the relative signs of the fields) and find

$$\frac{\partial A^{\mathrm{I}}}{\partial r^{\mathrm{I}}}=-59.4\times10^{-4}\ \mathrm{cm^{-1}\ \AA^{-1}}$$

and

$$\frac{\partial A^{\mathrm{II}}}{\partial r^{\mathrm{II}}}=-52.3\times10^{-4}\ \mathrm{cm^{-1}\ \AA^{-1}}.$$

It should be pointed out that because we have neglected other interactions such as the anisotropic hyperfine interaction and the limited accuracy of the strain measurements used to determine $\partial r_i/\partial P$, these numbers are at best accurate to $\pm20\%$.

One may argue that the change in Mn-F distances

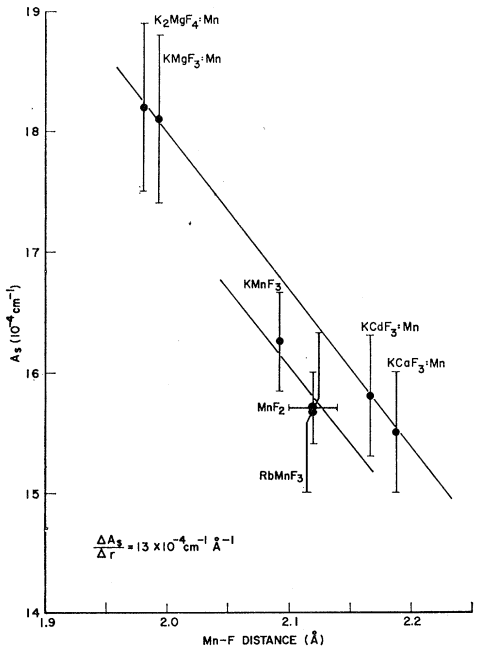

FIG. 19. The variation of the isotropic transferred hyperfine coupling constant with Mn-F distance for two types of systems: (1) Mn impurities in nonmagnetic cubic lattice hosts and (2) magnetically dense crystals containing Mn^{++} and F^-. The distortions of the crystal about the impurity results in the difference in magnitude of A's for these two systems at a given Mn-F distance. However, $\Delta A_s/\Delta r$ is the same for both systems. These data are taken from Shinji Ogawa, J. Phys. Soc. Japan **15**, 1475 (1960); M. B. Walker and R. W. H. Stevenson, Proc. Phys. Soc. (London) **87**, 35 (1966).

[38] G. B. Benedek and T. Kushida, Phys. Rev. **118**, 46 (1960).

over the pressure range considered is exceedingly small and thus not appropriate to the larger impurity-induced changes that we wish to consider. As a check on this, we have plotted in Fig. 19 the isotropic transferred hyperfine coupling constant in a number of materials versus their appropriate Mn-F distances.

The doped diamagnetic compounds all have the Mn^{2+} impurity in a cubic site, therefore, we expect any distortions of the lattice to be similar for all four compounds. As one can see, these distortions lead to a constant addition to all of the A_s values without changing the dependence of A_s on the Mn-F distance. From these data we find $\Delta A_s/\Delta r \simeq 13\times10^{-4}$ cm^{-1} Å^{-1}, a value radically different than the one obtained from the pressure studies. Even for this value of $\Delta A_s/\Delta r$, it is quite apparent that A_s is extremely sensitive to small change in Mn-F distance and thus strain effects.

While it is extremely difficult to quantitatively describe impurity-induced strains, we would now like to qualitatively discuss the strain effects first for the "dipolar" lines and then for the "hyperfine" lines.

Remember that of the four significantly shifted sites c, l, e, f, the agreement was excellent for sites c and e with systematic discrepancies for sites l and f. The discrepancies for a given site have the same sign which is probably due to MnF_2 having the largest lattice parameters of all the transition-metal fluorides.[39] In other words, the effective ionic radius for the impurities is always smaller than the Mn^{2+} effective ionic radius. Note also that the two sites exhibiting strain effects are close to a line parallel to the c axis, which passes through the impurity, while the other two sites are in the plane perpendicular to this line. This can be explained qualitatively by considering the following model. For an idealized lattice with the fluorine site symmetry shown in Fig. 2, we take $\phi=120°$; $r_I=r_{I'}=r_{II}$ and $A^I=A^{I'}=A^{II}$. Then the frequency shifts, neglecting the dipolar field, are

$$\Delta\nu_i=[\partial A/\partial r][\Delta r_I+\Delta r_{I'}-\Delta r_{II}]\langle S_z\rangle. \quad \text{(A5)}$$

If the strain is perpendicular to the plane defined by the four ions, then $\Delta r_I=\Delta r_{I'}=\Delta r_{II}\approx 0$. Thus, there is no frequency shift. If the strain is along the direction of r_{II} then

$$\Delta r_I=\Delta r_{I'}\approx\Delta r_{II}\cos(\phi/2)=\tfrac{1}{2}\Delta r_{II}.$$

Again, $\Delta\nu_i\approx 0$.

However, if the strain is along the direction of r_I, then $\Delta r_{I'}=\Delta r_{II}\approx\Delta r_I\cos(\phi/2)=\frac{1}{2}\Delta r_I$, and

$$\Delta\nu_i=[\partial A/\partial r]\langle S_z\rangle\Delta r_I.$$

Therefore, while the strain may be distributed isotropically about the impurity, only sites above and below the impurity will exhibit shifts due to this strain.

If this simple model has some validity we may further expect that Δr_I for sites f and l should be proportional to ΔC, Where ΔC is the difference in lattice constants in the C direction for pure MnF_2 and pure XF_2, when X is the impurity ion. We have plotted in Fig. 20 ΔC versus $\Delta\nu$ for sites f and l. The reasonably linear relations are further evidenced as to the nature of the additional shifts observed. In fact, movement of the Mn spins, immediately above and below the impurity, toward the impurity would yield the right sign to the shifts observed for lines l and f.

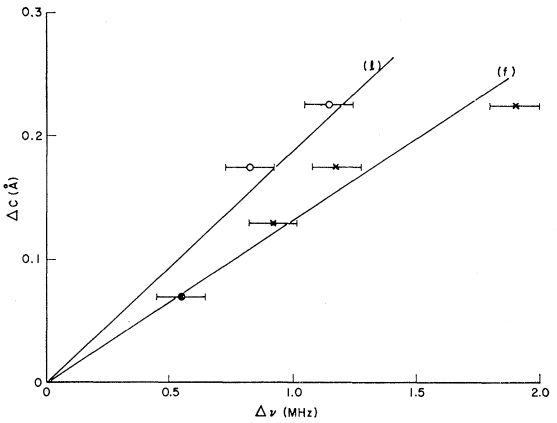

FIG. 20. The strain-induced frequency shifts $\Delta\nu$ for sites (l) and (f) in MnF_2:X are correlated with the difference in unit-cell dimensions ΔC in the [001] direction in the isostructural lattices XF_2 and MnF_2.

A more quantitative description of the strain effects requires a description of the distribution of strains around the impurity (i.e., how the lattice relaxes about the impurity).

Similarly, for the "hyperfine" lines we have

$$\Delta\nu^I=S_{\rm imp}\frac{\partial A^I(\rm imp)}{\partial r^I}\Delta r_I{}^{\rm imp}+S_{\rm Mn}\frac{\partial A^I(\rm Mn)}{\partial r^I}\Delta r_I - S_{\rm Mn}\frac{\partial A^{II}(\rm Mn)}{\partial r^{II}}\Delta r_{II}, \quad \text{(A6a)}$$

$$\Delta\nu^{II}=2S_{\rm Mn}\frac{\partial A^I(\rm Mn)}{\partial r^I}\Delta r_I - S_{\rm imp}\frac{\partial A^{II}(\rm imp)}{\partial r^{II}}\Delta r_{II}{}^{\rm imp}, \quad \text{(A6b)}$$

where Eq. (A6a) is intended for an impurity in a type I site and (A6b) for an impurity in a type II site (see Fig. 2). As the spins are known, one need only determine $\partial A^i/\partial r^i$ and Δr_i for the various sites. For the $\partial A^i/\partial r^i$ values we take those determined earlier from Fig. 19 (scaled by the appropriate spin value). These results are strictly valid only for pure MnF_2, however, due to the similarity in bond length and the similar amount of electron transfer in all of the XF_2 compounds, we will use these values appropriately scaled for the impurity as well. Estimating Δr_i for the various sites is a much more difficult task. Our model assumes the crystal is purely ionic. Any contributions of covalency or mag-

[39] J. W. Stout and R. G. Shulman, Phys. Rev. **118**, 1136 (1960).

netic interactions to the binding energy are neglected. We also assume that when an impurity is placed in the crystal, only the six nearest-neighbor fluorines readjust their positions. This limitation on the "relaxation" of the crystal is probably the most crucial one and, as one might expect, will lead to overestimation of the Δr_i values.

Following Pauling[40] we take for the potential at an F^- site (for simplicity)

$$V_i=\sum_j\left[\frac{z_iz_je^2}{r_{ij}}+\beta_{ij}B_0\frac{e^2}{r_{ij}{}^n}(r_i+r_j)^{n-1}\right], \quad \text{(A7)}$$

where the first term is just the Coulomb interaction between the ions and the second term approximates the repulsive potential resulting from overlap of the ionic wave functions, β_{ij} is a quantum-mechanical factor which is 0.75 for F^-F^- repulsion, ~ 1 for Mn-F repulsion, and ~ 1.25 for Mn-Mn repulsion. r_i and r_j are the crystal radii of ions at sites i and j. Since the Mn^{++} ions are much smaller than the F^- ions, we may neglect Mn-Mn repulsion, and Eq. (A7) becomes

$$V_i=\sum_j\frac{z_fz_je^2}{r_{fj}}+\sum_{j=+}\beta_+B_0e^2\left(\frac{(r_f+r_i)^{n-1}}{r_{ij}{}^n}\right)+\sum_{j=-}\beta_-B_0e^2\left(\frac{(2r_f)^{n-1}}{r_{ij}{}^n}\right). \quad \text{(A8)}$$

For the crystal to be stable one requires that the fluorine ion occupy a site of stable equilibrium. Thus, $\partial V_i/\partial X=0$, where X is a parameter indicating the deviation of bond length from the equilibrium value for pure MnF_2, and yields

$$0=\sum_j\frac{z_fz_je^2}{r_{ij}{}^2}\left(\frac{\partial r_{ij}}{\partial x}\right)+\sum_{j=+}n\beta_+B_0e^2\left(\frac{(r_f+r_i)^{n-1}}{r_{ij}{}^{n+1}}\right)\left(\frac{\partial r_{ij}}{\partial x}\right)+\sum_{j=-}\beta_-B_0e^2n\left(\frac{(2r_f)^{n-1}}{r_{ij}{}^{n+1}}\right)\left(\frac{\partial r_{ij}}{\partial x}\right). \quad \text{(A9)}$$

As we only wish an order-of-magnitude estimate, we make as many simplifying assumptions as possible. Thus we neglect F-F repulsion and assume the fluorines only move radially with respect to the impurity. Then the r_{ij}'s for the two fluorine sites may be written as follows:

$$\begin{aligned}&\text{type I:}\quad r_{\mathrm{I}}=r_0(1+\delta_{\mathrm{I}}),\\ &\qquad\quad r_{\mathrm{I}'}=r_0(1+\delta_{\mathrm{I}}\cos\phi),\\ &\qquad\quad r_{\mathrm{II}}=r_0[1-\delta_{\mathrm{I}}\cos(\phi/2)];\end{aligned} \quad \text{(A10)}$$

$$\begin{aligned}&\text{type II:}\quad r_{\mathrm{I}}=r_0[1-\delta_{\mathrm{II}}\cos(\phi/2)],\\ &\qquad\quad r_{\mathrm{I}'}=r_0[1-\delta_{\mathrm{II}}\cos(\phi/2)],\\ &\qquad\quad r_{\mathrm{II}}=r_0(1+\delta_{\mathrm{II}});\end{aligned} \quad \text{(A11)}$$

where $\delta\equiv x/r_0$ parametrizes the changes in X-F distance due to the impurity. Combining these expressions with Eq. (A9) and only keeping terms to first order in δ yields

$$\delta^{\mathrm{I}}=\frac{2(1+\cos\phi-\cos\tfrac{1}{2}\phi)-(n/R_0{}^{n-1})(b_i+b_h\cos\phi-b_h\cos\tfrac{1}{2}\phi)-2\Sigma_{\mathrm{I}}{}^{(2)}}{4[1+\cos^2\phi+\cos^2(\tfrac{1}{2}\phi)]-[n(n+1)/R_0{}^{n-1}][b_i+b_h\cos^2\phi+b_h\cos^2(\tfrac{1}{2}\phi)]+2\Sigma_{\mathrm{I}}{}^{(1)}} \quad \text{(A12)}$$

and

$$\delta^{\mathrm{II}}=\frac{2[1-2\cos(\phi/2)]-(n/R_0{}^{n-1})[b_i-2b_h\cos(\phi/2)]+2\Sigma_{\mathrm{II}}{}^{(2)}}{4[1+2\cos^2(\phi/2)]-[n(n+1)/R_0{}^{n-1}][b_i+2b_h\cos^2(\phi/2)]-2\Sigma_{\mathrm{II}}{}^{(1)}}, \quad \text{(A13)}$$

where ϕ is the angle defined in Fig. 2, b_i and b_h are the impurity and Mn^{2+} repulsive core parameters defined by

$$b_j=\beta_+B_0(r_f+r_j)^{n-1},$$

and $\Sigma^{(1)}$ and $\Sigma^{(2)}$ are the Coulomb interaction sums for all other sites but the three neighboring sites defined by

$$\sum_{j'}\frac{z_fz_je^2}{r_{ij}{}^2}\left(\frac{\partial r_{ij}}{\partial x}\right)=\Sigma^{(1)}\delta+\Sigma^{(2)}.$$

These sums have been performed explicitly by computer over approximately 4000 atoms. n may be determined from compressibility data.[41] The repulsive core parameters are determined by letting $b_i\rightarrow b_h$, thus $\delta\rightarrow 0$. As the denominators remain finite and nonzero, the numerators in Eqs. (A12) and (A13) must vanish. This leads to the expressions for b:

$$b=\frac{2R_0{}^{n-1}}{n}\left[1-\frac{\Sigma_{\mathrm{I}}{}^{(2)}}{1+\cos\phi-\cos(\phi/2)}\right]$$

and

$$b=\frac{2R_0{}^{n-1}}{n}\left[1+\frac{\Sigma_{\mathrm{II}}{}^{(2)}}{1-2\cos(\phi/2)}\right].$$

Therefore we may determine b_i by consideration of XF_2. Since n and ϕ do not change significantly from one ion fluoride to another, b must depend only on the equilibrium bond length:

$$\alpha\equiv 1-\left[\frac{\Sigma_{\mathrm{I}}{}^{(2)}}{1+\cos\phi-\cos(\phi/2)}\right]\approx\left[1+\frac{\Sigma_{\mathrm{II}}{}^{(2)}}{1-2\cos(\phi/2)}\right]=0.46.$$

[40] Linus Pauling, *The Nature of the Chemical Bond* (Cornell University Press, New York, 1960).

[41] Charles Kittel, *Introduction to Solid State Physics* (John Wiley & Sons, Inc., New York, 1953).

The equations for δ^{I} and δ^{II} may be written in numerical form:

$$\delta^{I}=\frac{1-(r_i/r_h)^5}{2.66-7(r_i/r_h)^5} \tag{A14}$$

and

$$\delta^{II}=\frac{1-(r_i/r_h)^5}{1-7(r_i/r_h)^5}. \tag{A15}$$

Using these expressions and Eq. (A6b) we determine for the Zn-II resonance a strain-induced frequency shift of $\sim$18 MHz compared to the observed value of $\sim$10 MHz. Evidently these small impurity-induced strains are more than sufficient to explain the observed shifts, however, a more comprehensive theory which properly includes the relaxation of the crystal and F^{-}-F^{-} repulsion appears necessary.

PHYSICAL REVIEW B VOLUME 1, NUMBER 7 1 APRIL 1970

Magnetic Phase Diagram of MnF_2 from Ultrasonic and Differential Magnetization Measurements

Y. SHAPIRA AND S. FONER
Francis Bitter National Magnet Laboratory, Massachusetts Institute of Technology, Cambridge, Massachusetts 02139*

(Received 12 December 1969)

The magnetic phase diagram of MnF_2, in the H-T plane, is determined in magnetic fields up to 200 kG directed along the [001] and [100] directions. The magnetic phase transitions appear as anomalies in the ultrasonic attenuation and/or the differential magnetization. Near the various second-order phase transitions, the attenuation of longitudinal sound waves exhibits λ anomalies, whereas near the spin-flop transition (which is a first-order transition) the ultrasonic attenuation exhibits a sharp spike and/or an abrupt increase, depending on the mode of propagation. The spin-flop transition is accompanied by a spike in the differential magnetic moment. The Néel temperature is $T_N=(67.33\pm0.03)$°K, and the triple point for $\mathbf{H}\|[001]$ is at $T_3=(64.9\pm0.1)$°K and $H_3=119\pm2$ kG. The field at the spin-flop transition (for $\mathbf{H}\|[001]$) increases monotonically with temperature from 92 ± 1.5 kG at 4.2°K to 119 ± 2 kG at the triple point. The curvature, at T_N, of the antiferromagnetic-paramagnetic boundary with $\mathbf{H}\|[001]$ is $d^2T/dH^2=-(3.2\pm0.2)\times10^{-10}$ °K/G^2. The curvature, at T_N, for the antiferromagnetic-paramagnetic boundary with $\mathbf{H}\|[100]$ is smaller by about an order of magnitude. The various phase boundaries are compared with the predictions of the molecular-field theory and other theoretical models.

I. INTRODUCTION

THE magnetic phase diagrams of antiferromagnets have been the subject of theoretical and experimental investigation in the last two decades. The earlier theoretical treatments,[1–4] which were carried out within the framework of the molecular-field approximation, established the general features of such phase diagrams. More recently, phase transitions in antiferromagnets have been treated using more sophisticated theoretical techniques.[5–8]

Experimental work on the phase diagrams of antiferromagnets has been limited by the unavailability of high magnetic fields. Notable exceptions are antiferromagnets with Néel temperatures in the liquid-helium range. Representative examples of work on antiferromagnets with relatively low Néel temperatures can be found in Refs. 9–14. Previous work on the phase diagrams of antiferromagnets with Néel temperatures above $\sim$10°K was largely confined to the spin-flop transition, which was investigated in several materials including MnF_2,[15–17] Cr_2O_3,[18,19] and α-Fe_2O_3.[20,21] However, the antiferromagnetic to paramagnetic transitions in MnF_2 were investigated by Heller in low fields

* Supported by the U. S. Air Force Office of Scientific Research.

[1] C. J. Gorter and T. van Peski-Tinbergen, Physica **22**, 273 (1956).

[2] C. G. B. Garrett, J. Chem. Phys. **19**, 1154 (1951).

[3] T. Nagamiya, K. Yosida, and R. Kubo, Advan. Phys. **4**, 1 (1955). The expression for $B_s'''(0)$ on p. 55 of this reference should be multiplied by 6.

[4] P. Heller, Phys. Rev. **146**, 403 (1966).

[5] H. Falk, Phys. Rev. **133**, A1382 (1964).

[6] F. B. Anderson and H. B. Callen, Phys. Rev. **136**, A1068 (1964).

[7] A. Bienenstock, J. Appl. Phys. **37**, 1459 (1966).

[8] J. Feder and E. Pytte, Phys. Rev. **168**, 640 (1968).

[9] H. M. Gijsman, N. J. Poulis, and J. van den Handel, Physica **25**, 954 (1959).

[10] W. van der Lugt and N. J. Poulis, Physica **26**, 917 (1960).

[11] V. A. Schmidt and S. A. Friedberg, J. Appl. Phys. **38**, 5319 (1967).

[12] J. H. Schelleng and S. A. Friedberg, Phys. Rev. **185**, 728 (1969).

[13] J. E. Rives, Phys. Rev. **162**, 491 (1967).

[14] H. Forstat, P. T. Bailey, and J. R. Ricks, Phys. Letters **30A**, 52 (1969).

[15] I. S. Jacobs, J. Appl. Phys. Suppl. **32**, 61 (1961).

[16] J. de Gunzbourg and J. P. Krebs, J. Phys. (Paris) **29**, 42 (1968).

[17] Y. Shapira and J. Zak, Phys. Rev. **170**, 503 (1968).

[18] S. Foner and S. L. Hou, J. Appl. Phys. Suppl. **33**, 1289 (1962).

[19] Y. Shapira, Phys. Rev. **187**, 734 (1969).

[20] S. Foner and Y. Shapira, Phys. Letters **29A**, 276 (1969).

[21] Y. Shapira, Phys. Rev. **184**, 589 (1969). Earlier work on α-Fe_2O_3 is quoted in this paper.